
Otto-von-Guericke University
Faculty of Electrical Engineering and Information Technology
Chair for Healthcare Telematics and Medical Engineering



Thesis

for obtaining the academic degree
Master of Science (M.Sc.)

Single Trial Decoding of Visual Spatial Attention Shifts from EEG and MEG Signals

Author:
Ardiansyah Pringgo Esmondo

February 28th, 2022

First Examiner:
Dr. rer. nat Stefan Dürschmid

Second Examiner:
Prof. Dr. rer. nat Georg Rose

Supervisor:
Dr. Christoph Reichert

Esmondo, Ardiansyah Pringgo:

*Single Trial Decoding of Visual Spatial Attention Shifts
from EEG and MEG Signals*

Master's Thesis, Otto-von-Guericke University
Magdeburg, 2022.

Abstract

Purpose Humans are constantly shifting their attention from one item to another. It has always been found that during a visual search task where attentional processing discriminates target and distractors, a particular event-related potential (ERP) component is elicited, known as N2pc. This thesis investigates whether visual-spatial attention shifts can only be extracted from a grand ERP average or decoded from a single trial.

Method To investigate the decodability at the single-trial level, binary classification of the EEG and MEG signals associated with the spatial attention shifts was employed by predicting the position of the attended target. The decoding accuracy is the number of correctly predicted target classes out of all the predictions. Implementing a spatiotemporal filter (STF) and generating combined trial datasets were included in the classification to increase the signal-to-noise ratio (SNR).

Results The obtained decoding accuracy reflected that the EEG and MEG associated with the N2pc were reliable to be decoded at the single-trial level. Mean decoding accuracy was reported to be higher with STF implementation and constantly increased as more combined-trial datasets were added. At the single-trial level, the mean decoding accuracy of EEG and MEG was 67.9% and 68.8%, respectively, and with STF implementation was 73.2% and 69.5%, respectively.

Conclusion Stronger discriminability to a relevant item among distractors in both visual fields could lead to more reliable N2pc in a single trial EEG/MEG, which drives better decoding performance.

Keywords Event-related Potentials, Attention shifts, N2pc, Selective Attention, Decoding, Classification, Support Vector Machine, Electroencephalography, Magnetoencephalography.

Task of the Thesis in the Original:



FACULTY OF
ELECTRICAL ENGINEERING AND
INFORMATION TECHNOLOGY

Task Description of a Master Thesis

Ardiansyah Pringgo Esmondo

Student ID: 221253

Topic

Single Trial Decoding of Visual Spatial Attention Shifts from EEG and MEG Signals

Task Description

In search displays humans can rapidly detect a target object located among distracting nontarget objects. Depending on the position in the visual field, the shift of attention to the target object is indexed by characteristic event related potentials (ERPs) as measured by electroencephalography (EEG) and obtained after averaging many repetitions of the stimulus. However, detecting these small interhemispheric differences on a single trial basis is challenging. Using EEG, it has been shown that averaging at least 3 repetitions of the stimulus is required to achieve an accuracy suitable to control a brain-computer interface. Magnetoencephalography (MEG) is the magnetic analogue to EEG, but provides complementary signals and a higher spatial resolution, which has been shown to reveal higher decoding accuracies in classification tasks.

The task of the student is to investigate the ability to decode from single trial EEG and MEG data in which visual hemifield a target object was shown. Two data sets will be provided for analysis. One of the datasets was already used for a different MEG study which has been published. The student will implement a decoding algorithm using adequate classification approaches. In the thesis the student will demonstrate how accuracy is changing when several trials are averaged and determine the accuracy as a function of trials involved. The results obtained by MEG data will be compared with the results obtained by simultaneously recorded EEG. Furthermore, the focus level was occasionally requested during the experiments. The student will investigate how the focus ratings correlate with the discriminability of trials.

Therefore, this thesis aims to find the answer of how does visual spatial attention shifts in EEG and MEG provide useful information for future brain-computer interface (BCI) studies. In a final analysis, the student will investigate the cause of failed behavioral responses, i.e. the unsuccessful processing of the stimuli, by predicting the attention shift according to the developed decoder.

Magdeburg, 03.09.2021

Start of thesis work: 11.10.2021
Date of submission: 28.02.2022

1st Examiner: Dr. rer. nat. Stefan Dürschmid

2nd Examiner: Prof. Dr. rer. nat. Georg Rose

1st Examiner

Prof. Dr. rer. nat. Georg Rose
(Chairman of Examination Board)

Declaration by the candidate

I hereby declare that this thesis is my own work and effort and that it has not been submitted anywhere for any award. Where other sources of information have been used, they have been marked, directly or indirectly.

The work has not been presented in the same or a similar form to any other testing authority and has not been made public.

Magdeburg, February 28th, 2022.
Esmondo, Ardiansyah Pringgo

Acknowledgements

First and foremost I would like to thank and express my profound appreciation to all my supervisors for their guidance in the last 15 months. To Dr. rer. nat Stefan Dürschmid for the best opportunity and believing in me to work on this thesis. To Dr. Christoph Reichert for patiently guiding me throughout the coding process. To Prof. Dr. rer. nat Georg Rose as a representative from the faculty and for his helpful insights in the process of this thesis.

I would like to express my deepest gratitude for my father, mother and younger sister for all their financial, mental and spiritual support. I am grateful for all their hard work and continuous prayer and I hope I have made them proud. I want to thank my beloved and closest friend, Amanda Soengadie for always being honest, supportive, and having faith in me.

I would like to thank Sigrid Schmidt and Gisela Münch, my sweetest and kindest friends from Rostock who continually believed in me and support me since day one I moved to Magdeburg. Last but not least, thank you to my colleague Seyedeh Razavizadeh for all the guidance, insights, advice and for being a great discussion partner; Istiaque Amin for his helpful advice on how to approach this thesis from the writing process to the very last process of defending this thesis; Yohana Junitama Kustita for their help at the very last minute; all my friends in Magdeburg and the Indonesian community that I can not mention one by one for their support and kindest prayers throughout the years.

Contents

Abstract	i
Declaration	iii
Acknowledgements	iv
List of Figures	vii
List of Tables	viii
List of Acronyms	ix
1 Introduction	1
1.1 Motivation	1
1.2 Goals	2
1.3 Structure of Thesis	2
2 Literature Review	3
2.1 EEG and MEG	3
2.2 Event-Related Potentials	4
2.3 Visual Attention Shifts Component	6
2.4 Classification in BCI	8
2.5 Canonical Correlation Analysis	8
3 Related Works	10
3.1 Single-trial Decoding	10
3.2 N2pc Decoding Algorithm with Classification	10
3.3 N2pc Decoding Algorithm with Spatial Filtering	11
3.4 Combining ERP Trials for Classification	11
3.5 Mind-wandering and N2pc	12
4 Method	13
4.1 Dataset	13
4.1.1 Participants and Recordings	13
4.1.2 Experimental Paradigm	14
4.1.3 Dataset Preparation	15
4.2 Preprocessing	15

4.3	Spatial Attention Shift	16
4.3.1	N2pc from ERP	17
4.3.2	N2pc from ERF	17
4.4	Decoding Algorithm	17
4.4.1	SVM Classifier	18
4.4.2	K-Fold Cross-Validation	20
4.4.3	Spatio-temporal Filters Estimation for Classification	21
4.4.4	N-Combined Trial Sets	22
4.4.5	Evaluation Metrics	22
4.5	Analysis of the Decodability	23
4.5.1	Significance Test for Decoding	23
4.5.2	Decoding Performance Towards Incorrect Trials	23
4.5.3	Decoding Performance Comparison with a Published Dataset	24
4.5.4	Focus Rate and Decoding Accuracy Correlations	24
5	Results	25
5.1	Decoding Performance of Single-Trial	25
5.2	Decoding Performance in Different Conditions	25
5.3	Decoding Performance Comparison with a Published Dataset	27
5.4	Focus Level and Decoding Accuracy Correlations	28
5.5	N2pc Extraction Results	29
6	Discussion	32
6.1	Outcome	32
6.2	Limitation and Future Work	34
7	Conclusion	35
Bibliography		36
Appendix		45

List of Figures

2.1	Brain Signals Recording Setup.	3
2.2	The Current Dipole Source of MEG and EEG [27, Ch.1]	4
2.3	ERP Recording Using The Oddball Paradigm [13, Ch.1].	5
2.4	Grand Average EEG [13, Ch.1].	6
2.5	A common N2pc paradigm (upper) and its corresponding grand average ERP waveforms (lower) from posterior occipitotemporal electrode sites [31, 42].	7
4.1	Single-trial paradigm with a focus question [4].	14
4.2	Continuous recording into epochs (the signal figure was taken from [69]).	15
4.3	Preprocessing block diagram.	16
4.4	The structure of predictor and labels.	18
4.5	Hyperplane in Support Vector Classifier	19
4.6	Decoding Algorithm Pipeline.	20
5.1	Decoding Performance of 13 Participants in Single-Trial Level.	26
5.2	Mean Decoding Accuracy of EEG and MEG.	27
5.3	Mean Decoding Accuracy Trend of Correct and Incorrect Trials.	28
5.4	Mean Decoding Accuracy of MEG.	28
5.5	Correlation Between Decoding Accuracy and Mental State Ratings	30
5.6	Grand Average of ERP and ERF.	31

List of Tables

4.1	Confusion Matrix of Binary Classification [84]	22
5.1	Mean decoding accuracy of EEG and MEG	27
5.2	Mean decoding accuracy of current and published MEG datasets	29
A.1	Decoding Accuracies of 13 Participants at Single-trial Level (n=1)	45
A.2	Decoding Accuracies of 13 Participants (n=2)	45
A.3	Decoding Accuracies of 13 Participants (n=3)	46
A.4	Decoding Accuracies of 13 Participants (n=4)	46
A.5	Decoding Accuracies of 13 Participants (n=5)	47
A.6	Decoding Accuracies of 13 Participants (n=6)	47
A.7	Decoding Accuracies of 13 Participants (n=7)	48
A.8	Decoding Accuracies of 13 Participants (n=8)	48
A.9	Decoding Accuracies of 13 Participants (n=9)	49
A.10	Decoding Accuracies of 13 Participants (n=10)	49
A.11	Parieto-occipital channels of EEG and the corresponding N2pc period. The temporal N2pc activity was defined by the significant difference between contralateral and ipsilateral waveforms (grey shade in Figure 5.6a)	50

List of Acronyms

BCI Brain-Computer Interface

CCA Canonical-Correlation Analysis

EOG Electrooculography

EEG Electroencephalography

ERP Event-Related Potential

ERF Event-Related Field

hEOG Horizontal Electrooculography

LVF Left Visual Field

MEG Magnetoencephalography

MW Mind-Wandering

N2pc N2-Posterior-Contralateral

RVF Right Visual Field

SNR Signal-to-Noise Ratio

STF Spatio-temporal Filter

SD Standard Deviation

SVM Support Vector Machine

TPR True Positive Rates

vEOG Vertical Electrooculography

1 Introduction

1.1 Motivation

In any crowded environment, the challenges in processing selective attention are eliminating non-necessities and coordinating our attention to the objective-related object. Humans can rapidly identify a target object scattered among distracting non-target objects in a visual search display where various objects compete for attention [1]. Depending on the position in the visual field, spatially shifting the attention to the target object is composed of characteristic event-related potentials ERPs as measured by electroencephalography (EEG) [2, 3].

The human mind continuously shifts from wandering away out of the conscious perception of the external environment to focusing on their internal environment in their daily life. As a result, humans have to put more effort into countering this circumstance to maintain a good performance in an experimental task. A recent visual search experiment from *Wienke et al.* assessed neural response when participants covertly shifted their spatial attention to related target stimuli [4]. They found that the ERP component called N2pc as a neural marker of attentional selection [2, 5–7] was higher in amplitude during mind-wandering (MW) phases [4]. Higher N2pc amplitude has been linked to greater attention on the relevant target item or distractor suppression in numerous previous studies (see for example [6, 8]).

In typical ERPs experiments, the obtained neural signals from participants were averaged across many experimental trials containing stimuli to increase the signal-to-noise ratio (SNR). The ability to detect the small interhemispheric difference from a single trial is still unclear and challenging. One previous EEG study has shown that at least averaging three repetitions of trial has achieved accuracy suitable to control brain-computer interface BCI [9]. The ERP has the characteristic of having excellent temporal resolution but limited spatial resolution due to volume conduction by the skull [10–12]. Magnetoencephalography (MEG) as the magnetic analog of EEG [13, Ch. 2] provides more excellent spatiotemporal resolution [14].

Compared to numerous EEG-based BCI experiments, only a few BCI studies have incorporated the MEG, despite its advantage and feasibility in BCI [15]. Offline investigation revealed that the classifier based on support vector machine (SVM) performed well with MEG [16]. A study with simultaneous recording of EEG and MEG associated with finger movements revealed that decoding accuracy in classification tasks is greater in MEG than EEG [17]. However, the use of single-trial ERP decoding through classification is rarely developed, specifically on visual-spatial attention shifts.

Given the recent finding of visual-spatial attention shifts, this study will unravel the ability

to decode the N2pc as the marker of attentional shifts from single-trial EEG and MEG data in which the visual hemifield of a target object was shown.

1.2 Goals

This thesis aims to find the possible solution to the following research question:

“How many visual-spatial attention shifts can be correctly decoded from EEG and MEG data on a single trial level for future BCI applications?”

For this purpose, this thesis applies a decoding algorithm using an adequate classification approach. In the classification process, spatial filters are applied as a performance enhancer. In addition to single-trial accuracy, several trials are averaged to determine the accuracy of combined trial sets. Ultimately, the results from MEG data and the simultaneously recorded EEG are compared. The focus ratings are associated with trials discriminability to study the relationship between the behavioral responses from the experimental paradigm and the decoding outcomes. At last, investigate the cause of failed behavioral responses, i.e., unsuccessful processing of the stimuli.

1.3 Structure of Thesis

The chapters of this thesis are mentioned below.

- Chapter 2: Literature Review

This chapter will provide the appropriate theoretical context for the study by reviewing the literature from relevant fields.

- Chapter 3: Related Works

The related research, which offers a state-of-the-art approach, will be discussed in this chapter.

- Chapter 4: Method

In this chapter, the conventional and newly proposed methods will be discussed.

- Chapter 5: Results

Here all the final results of the proposed approach are presented.

- Chapter 6: Discussion

The final results and the implications will be discussed in detail.

- Chapter 7: Conclusion

As the final chapter, the findings of the thesis will be concluded.

2 Literature Review

The purpose of this chapter was to provide readers with a basic understanding of the study's theoretical foundations by delivering an overview of relevant literature. Specifically, some essential aspects are associated with the visual attentional shifts studies and how these components can be decoded with a machine learning approach.

2.1 EEG and MEG

The human brain receives continuous information about the scene in the surrounding environment at every moment, conscious or unconsciously. Its function includes controlling thought, memory, vision, emotion, motor skills, breathing, making decisions, and most body activities [18]. These are done through billions of neurons in the brain that receive, encode, and distribute information in the nervous system. Each neuron is driven by electrical currents that travel and interact with neighboring neurons through chemical signals sent back and forth [19]. Thus, monitoring and recording brain dynamics through electrical impulses is feasible.

Hans Berger in 1929 first invented a classical approach in recording human brain electrical activity called an EEG. It tracks electrode electric activity from the scalp surface and observes the generalized activity changes in the cerebral cortex over time [22]. Since then, EEG has

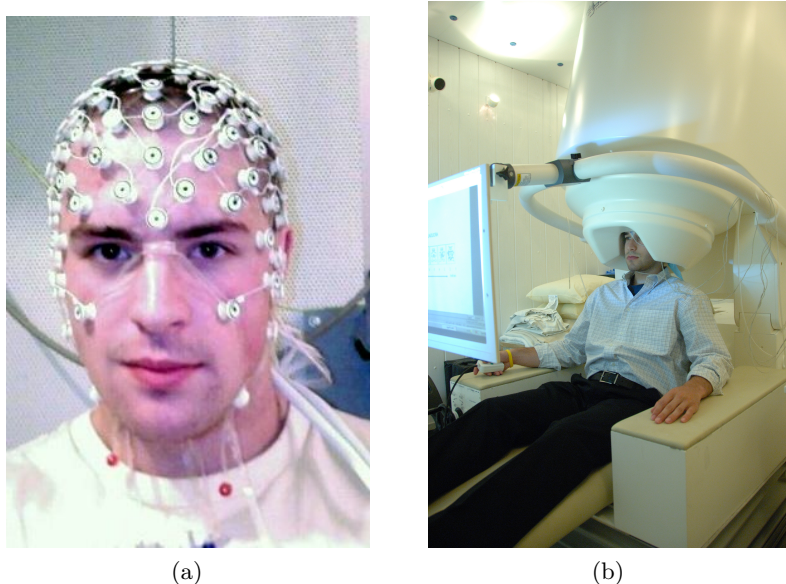


Figure 2.1: Brain Signals Recording Setup.

- a) A participant is wearing an EEG device. [20], b) A participant is doing an MEG experiment in a magnetically shielded room. [21].

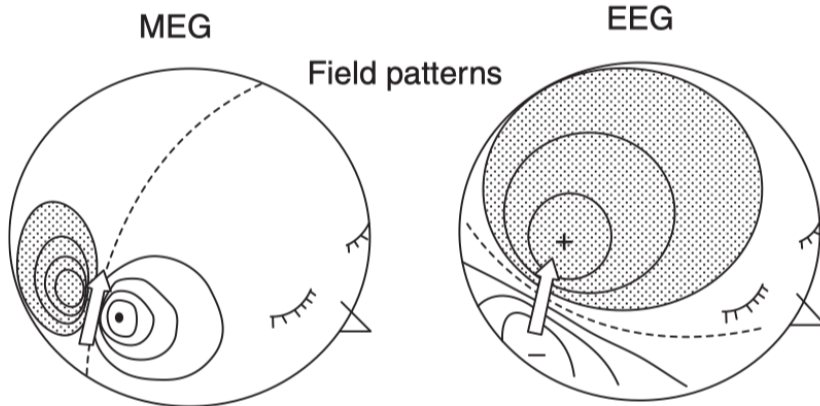


Figure 2.2: The Current Dipole Source of MEG and EEG [27, Ch.1]

- . The MEG (left) shows magnetic flux flowing out of the head, and the dark area is positive concerning the rule of thumb. The EEG (right) shows the positive electrical potential.

advanced significantly and is now the preferred data collection method in biomedical applications due to its high temporal resolution, less expensive, and non-invasive nature. It is also widely used in neuroscience research, including motor, cognitive, neuroimaging, and brain-computer interface (BCI) [23]. However, EEG also suffers from disadvantages, e.g., low signal-to-noise ratio (SNR) [24] and low spatial resolution [25, Ch.1]. Another alternative way to record the electrical activity from the brain is with MEG. MEG is a non-invasive measurement of the magnetic field produced by neuronal electrical activity that provides very high temporal resolution and excellent spatial resolution. Electric currents and magnetic fields are basically interlinked, perpendicular to the current direction (see Figure 2.2) [14]. This interconnection makes MEG unaffected by the issues often produced by intermediary processes such as neurovascular coupling in functional magnetic resonance imaging (fMRI) or functional near-infrared spectroscopy (fNIRS) [26].

2.2 Event-Related Potentials

EEG and MEG could measure and record the complex brain electrical activity that assembled many neural and non-neural activity sources. The electrical activity unrelated to any particular sensory or motor outputs such as alpha and sleep rhythms is called spontaneous potentials. On the other hand, evoked potentials are instantaneous responses to external stimuli such as a blinking light or a beeping sound [25, Ch.1] [28, Ch.5]. Evoked potentials are sometimes also termed event-related potentials (ERPs) but usually with higher latency and higher cognitive processing [29].

ERP basically represents the evaluated brain response that results directly from a particular sensory, cognitive, or motor event [13, Ch.1]. The magnetic counterparts to the ERP are called event-related fields (ERFs) [30]. The ERP signal pattern differs in polarity, amplitude, and length as a sequence of positive and negative peaks, as a sum of many action potentials that are time-locked to particular internal or external events, e.g., cognitive events or repetitive stimuli sequences (oddball paradigm) [31]. See Figure 2.3 for an illustration of how ERP is obtained in

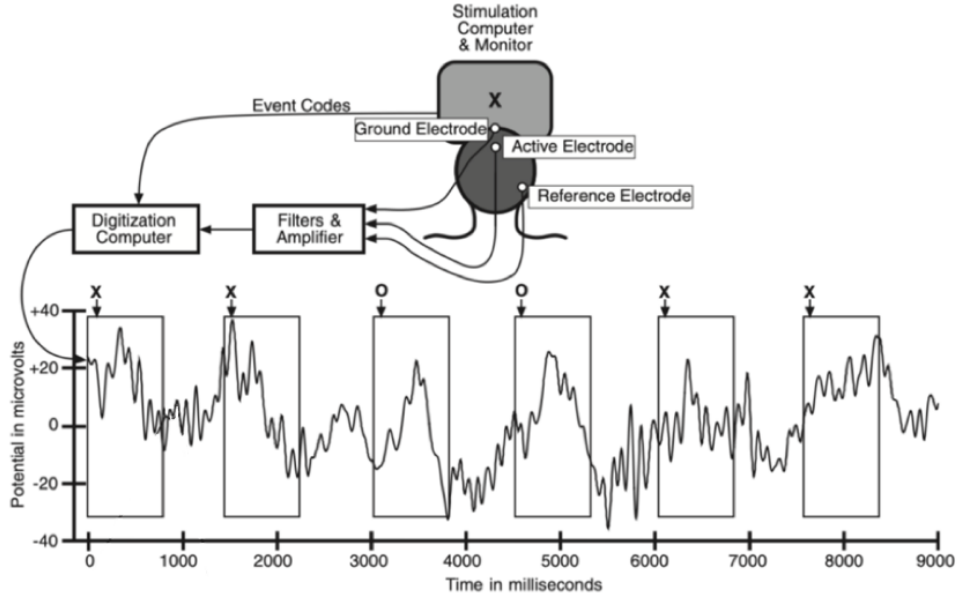


Figure 2.3: ERP Recording Using The Oddball Paradigm [13, Ch.1].

general. ERP is comparatively small compared to the raw EEG and is merged into the EEG signals and noises. Therefore, ERP cannot be detected without further treatment. By averaging many signals throughout the trials (see Figure 2.4), ERP can be observable, which are constantly produced by repetitive stimuli. It is expected that any brain function that is unassociated with the stimuli would balance each other out on specific trials and will lead to zero results in the averaged data [13, Ch.1].

ERP research entered a new phase with the first finding of cognitive ERP component called contingent negative variation (CNV) by *Walter et al.* [32]. In an experimental setting where participants were shown repetitive target stimuli and a prior warning of the cue, it was found that the CNV was elicited as a negative deflection at the moment between the cue and the response of the participants to the target. The CNV component was then known as the anticipatory effect [33]. This finding influenced many researchers to explore more ERP components from other cognitive responses. *Kappenman and Luck* generalized the definition of ERP component as a fragment that corresponds to a particular brain or psychological mechanism [34]. ERP components are commonly indicated by P (positive) or N (negative) peak followed by either a number designating the waveform's peak latency or its ordinal location (e.g., N400 is a negative component peaking at 400ms, and P2 is the second prominent positive peak) [13, Ch.3]. ERP components are classified into three types: (1) Exogenous, which are reliant on the presence of sensory input; (2) Endogenous, which represent fully task-dependent brain processes; (3) Motor, which must accompany the planning and execution of a specific motor response [35]. One of the most used endogenous ERP components was discovered by *Sutton et al.*, namely P3 or P300 [36]. P300 is commonly explored with the oddball paradigm and elicited as a positive deflection around 300ms after a stimulus [37]. It has been widely considered that P300 was associated with attentional and memory mechanisms [38]. In BCI applications, P300 was first

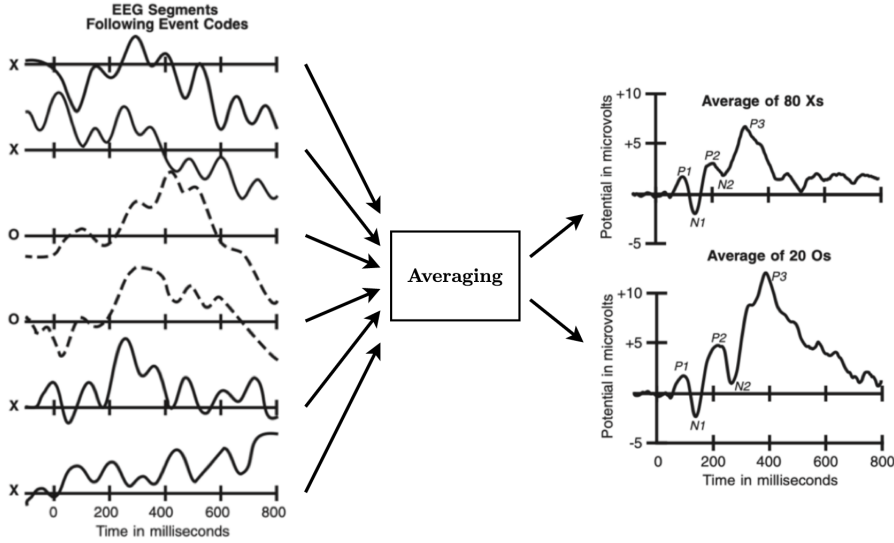


Figure 2.4: Grand Average EEG [13, Ch.1].

By averaging epoched EEG across trials, ERP with high SNR can be observed, showing prominent peaks of ERP components.

utilized as communication control (speller) by *Farwell and Donchin* [39], and since then has been used extensively.

2.3 Visual Attention Shifts Component

During wakefulness, we receive immense sensory input from our surroundings at any given time. To precisely select the relevant information, our attention should be allocated to the visual scene. According to the review by *Carrasco*, there have been growing studies about visual attention since 1980. It has been shown that directing attention to a spatial location or to distinguishing features of a target can enhance its discriminability and the evoked neural response. Research showed that focusing attention on a spatial spot (spatial attention) or identifying characteristics of an object (feature-based attention) can improve the evoked neural response and discriminability. Spatial attention can guide an observer to a specific location with eye movements (overt) or without eye movements (covert) [40].

Numerous studies have suggested that an electrophysiological pattern of visual attention reflects the same type of attentional-related processing indexed by a specific ERP component, namely the N2-posterior-contralateral (N2pc). The N2pc is a part of the N2 subcomponents family, which is susceptible to competition between the target and distractors, seen as a negative-going voltage deflection recorded at posterior EEG channels contralateral to the target (compared to ipsilateral) roughly between 200ms and 300ms after stimulus onset [1–3, 35]. Specifically, the N2pc is elicited after covert attention is focused on the peripheral targets in the visual field and associated with spatially selective attentional processes [2, 3, 5, 33, 41].

In a visual search task, the N2pc is often used as a neural marker to track spatial attentional

selection towards a target item among distractors. An example by [43] where N2pc was used to measure visual and spatial working memory to investigate the working memory influence on task performance of different adults by adapting visual search task employed in [42, 44]. The visual search task represented how a general N2pc paradigm was conducted (see the upper part in Figure 2.5). According to *Steven J. Luck*, the paradigm consisted of arrays of stimuli in many trials of a 5-minutes block with a target indication at the beginning of each block. Each stimulus array comprised one red square, one green square, and was surrounded by black distractor squares. The orders of the colored squares changed across trials and were always on opposing sides of the display. The observer must select one of two targets for each array to specify if the target shown in the attended color has a top or bottom opening. The subject would focus on an item in the left visual field (LVF) if red were the target color and the right visual field (RVF) if green were the target color.

The respective grand average ERPs from the paradigm were illustrated in the lower part of Figure 2.5. The N2pc can be seen as a more negative voltage when the attended target is contralateral to the electrode site (average of RVF target to the left hemisphere and LVF target to the right hemisphere) than when the attended target is ipsilateral (average of LVF target to the left hemisphere and RVF target to the right hemisphere). Collapsing the LVF/RVF targets and the left/right hemispheres to create contralateral and ipsilateral waveforms could reduce overall discrepancies. The N2pc can be isolated by subtracting ipsilateral from contralateral waveforms. It often takes place within the N2 wave time range (200–300ms) and is detected at posterior scalp sites over the visual cortex (i.e., occipito-temporal areas), with a peak voltage around the PO7 and PO8 electrodes [31].

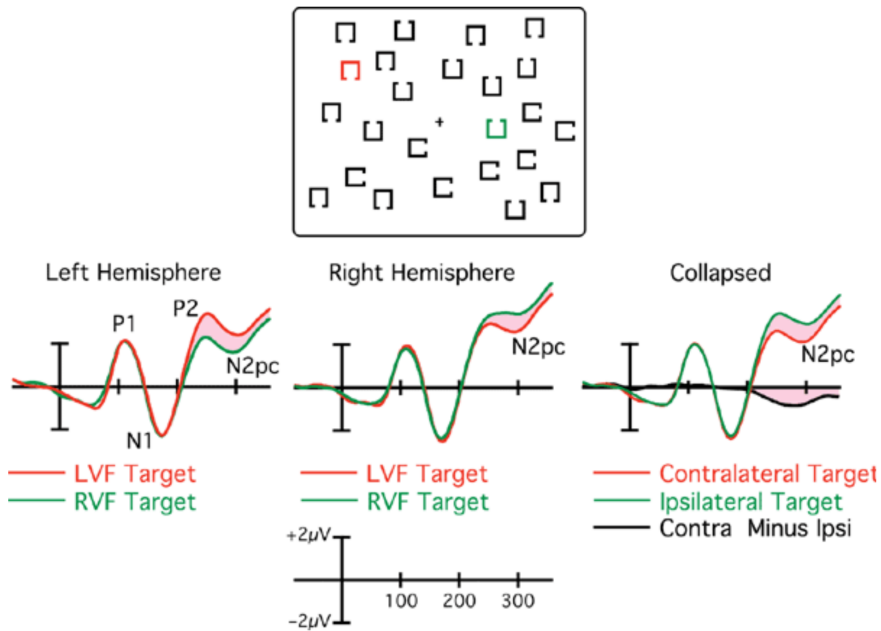


Figure 2.5: A common N2pc paradigm (upper) and its corresponding grand average ERP waveforms (lower) from posterior occipitotemporal electrode sites [31, 42].

2.4 Classification in BCI

As part of the statistic and machine learning, a type of predictive learning problem in which an outcome label is predicted for a given input data sample is called classification [45]. In most cases, the outcome measurements (class labels) are quantitative or categorical. They will be trained with a set of data that includes features to build a predictive model or learner that allows us to predict the outcome of new unseen data, and a good model can predict the outcome accurately. This is called supervised learning because the labels can guide the learning procedure. When the labels do not exist, and the learning process only relies on features observation, it is called unsupervised learning [46, Ch.1].

The research involving brain signal classification has consistently increased, especially in BCI studies. Researchers have always seen that brain activity or other electrophysiological measures could provide non-muscular electrical signals that could be exploited to send messages or communicate with the external or internal environment [47]. This ongoing interaction is the basis of the definition of BCI. Mainly EEG is the preferred method for signal acquisition [48] because it tends to be more portable, easy to use, and inexpensive than other recording techniques. Most importantly, it can be beneficial for the study involves severely paralyzed participants, e.g., communication tool assistant for ALS patients [49], wheelchair control with [50], stroke rehabilitation [51]. These are BCI applications resulting from the command translated from the classified EEG features.

According to *Lotte et al.*, the BCI system is supposed to be an online closed-loop. However, the offline procedure is also worth noting, essentially how the obtained EEG is decoded to get a reliable system, and the classification algorithm takes place in this step [48]. There were numerous classification methods applied in BCI. *Lotte et al.* provided some comparisons between the classifier and guidelines to choose a suitable classifier depending on the context. It was found that the SVM classifier was adequate for the synchronous type of BCI. This is mainly due to regularization, low variance, and robustness concerning curse-of-dimensionality [52, 53].

2.5 Canonical Correlation Analysis

Canonical correlation analysis (CCA) was first discovered by *Hotelling* [54]. It is a multivariate statistical method and used when there are two sets of data, which may have some underlying correlation. CCA can be used to find linear transformations for these two datasets, such that the correlation between the two canonical variables is maximized. Assuming two multidimensional datasets $\mathbf{X} \in \mathbb{R}^{n \times c}$ and $\mathbf{Y} \in \mathbb{R}^{n \times d}$ of c and d variables ($c \geq d$) and n observations, and their linear combinations $\mathbf{U} = \mathbf{XW}_x$, $\mathbf{W}_x \in \mathbb{R}^{c \times d}$ and $\mathbf{V} = \mathbf{YW}_y$, $\mathbf{W}_y \in \mathbb{R}^{d \times d}$, respectively [55].

According to [56] and [57] explanation, CCA finds the two transformations \mathbf{W}_x and \mathbf{W}_y , which maximize the canonical correlation ρ_i^* between the canonical variables \mathbf{U}_i and \mathbf{V}_i

$$\rho_i^* = \frac{cov(\mathbf{U}_i, \mathbf{V}_i)}{\sqrt{var(\mathbf{U}_i)var(\mathbf{V}_i)}}. \quad (2.1)$$

\mathbf{W}_x and \mathbf{W}_y linear transformations are chosen to equal one deviation, though unrelated to the other canonical variables

$$var(\mathbf{U}_i) = var(\mathbf{V}_i) = 1 \quad (2.2)$$

$$cov(\mathbf{U}_i, \mathbf{V}_j) = cov(\mathbf{U}_j, \mathbf{V}_i) = 0, \forall i \neq j. \quad (2.3)$$

3 Related Works

The utilization of visual-spatial attention shifts marked by N2pc has not been widely used for BCI applications. Specifically for decoding the spatial or temporal information from the recorded signals. However, some studies have attempted to decode the N2pc from EEG and/or MEG, which may be regarded as a state-of-the-art method in this field of study.

3.1 Single-trial Decoding

Non-invasive brain imaging techniques such as EEG and MEG have historically served as a tool for comparing and contrasting mean values across conditions or groups of subjects. Modeling the single-trial mechanism of the human brain can be referred to as neural pattern classification or decoding. Given how far the field has developed, it is possible to go beyond such averaging with single-trial analysis or decoding by looking at how trials vary from one another. As it turns out, single-trial analysis can reveal previously unobservable information [58]. However, decoding a single-trial of a brain mechanism tends to be intricate due to trial-to-trial variability and artifacts. *Blankertz et al.* provided a state-of-the-art recommendation for classifying ERP components to which the features selection for classification were adapted in our method [59]. Essentially, ERPs are composed of temporal evolution associated with their spatial distributions as they are recorded from many channels over time. Thus, spatio-temporal features were opted for the single-trial decoding.

3.2 N2pc Decoding Algorithm with Classification

The N2pc component of ERP has been discussed in various EEG and MEG studies to understand the underlying brain mechanisms [7, 60–62]. Especially as a measure of feature-based selection attention [31]. In the study of *Fahrenfort et al.*, N2pc as a feature-based attentional selection was utilized as a tracker to decode the position of the attended target stimulus, which cannot be accomplished using conventional N2pc methodology. Commonly, the N2pc component can only be analyzed by collapsing the ERP of the relevant target from the visual task and then applying the contralateral-minus-ipsilateral waveform of the attended target. One type of multivariate analysis from their study was called the backward decoding model (BDM) [63].

BDM used a linear discriminant classifier with 10-fold cross-validation to predict which relevant stimulus (e.g., a target at a specific position) was present based on EEG activity patterns. The datasets were divided into 10 equally subsets after the trial sequence was randomized. Using EEG amplitude at each electrode as features, the classifier was trained on 90% of the data to distinguish between classes and then tested the remaining 10%. This process was performed 10

times until every data was tested once. The average number of correct class assignments for each subject was then averaged over the ten folds. If the classification accuracy is above the chance level, the EEG signals exhibit the prediction [63]. Their decoding approach was constructed for every time point in a trial, resulting in the time course of classification accuracy, closely matching the time course of N2pc. However, their decoding approach was adapted and modified in this thesis to correspond to the objective of the thesis.

3.3 N2pc Decoding Algorithm with Spatial Filtering

According to *Reichert et al.*, the N2pc was considered an excellent tool for BCI command, especially if the BCI used covert shifts mechanism from the brain for control. However, there was no BCI solution where the user actively controls the system and receives feedback showing that their attention shifts have been recognized. Consequently, they offered a closed-loop BCI involving covert shifts decoding from EEG signals. In their visual paradigm, 12 visual stimuli sequences were presented. The participants were asked to move an avatar to a specific location by shifting the focus on a cued-colored target item (among other three colored items) that appeared in the LVF or RVF. The four colored items corresponded to a specific movement direction (blue/left, red/up, yellow/right, green/down). Once all essential EEG data had been sent to the BCI computer, feedback was generated with the avatar moved in a particular direction in response to the decoding algorithm. The decoding approach was driven by assuming that each color has a distinct left/right presentation sequence correlated to the lateralized disparities in hemispheric ERPs. Thus, the decoder tried to discover the best left/right presentation sequence to match the brain response [64].

The decoder was built using Canonical Correlation Analysis (CCA) and was modified to automatically estimate the best spatial weighting of channels while also estimating the time course of ERPs in substitute channels, which is closely related to the more recent study in [65]. The initial iteration of this method was published in [55], which demonstrated that appropriate spatial filtering significantly increases ERF detection accuracy, and [66] validated its performance in a P300-based closed-loop BCI with EEG and MEG. Instead of using the CCA-based spatial filter as a decoder alone, the spatial filter estimation was adapted in this thesis as a supplementary technique for classification.

3.4 Combining ERP Trials for Classification

Awni et al. evaluated the applicability of the covert attention BCI paradigm by examining participant classification performance using data gathered during an N2pc evoked task designed in [67]. The classification performance was assessed in the function of channel choices and the number of ERP trials (repetitions). Due to the noisy nature of ERP signals, it is unlikely that the N2pc would be appropriately identified in a single trial. Thus, it is common practice to combine multiple repetitions to enhance SNR. Classification feature was acquired from mean ERP voltage at significant difference time range. The first classification was analyzed across participants and the second within participants, using LDA. Across participants: the training and testing set

(from the whole dataset) composed of n randomly selected trials ($n = [1..12]$) which were then averaged. Within participants: As the number of trials became limited, the n -combined trials for training and testing were set to $n = [1..3]$ only. The best channel combinations were tested to get the best classification performance. Each classification procedure was repeated 500 times [9].

The results demonstrated that N2pc could be classified with reasonable accuracy. However, the performance was subject-dependent, i.e., differed among individuals. Using three combined trials, two individuals obtained an accuracy of over 75% across eight channels, while one person reached an even higher accuracy of over 90% using the optimum set of electrodes. It is likely that these differences were related to the easiness to detect N2pc response but could also be caused by other factors. Lastly, the authors suggested that future studies should acquire more trials for each participant, as the classification performance for the combined dataset with higher repetitions was improving [9]. Consequently, this thesis adapted the approach by involving $n = [1..10]$ repetitions as the combined trial set in classification, and the process was only repeated 10 times due to limited computational work.

3.5 Mind-wandering and N2pc

This thesis was highly connected to the study of *Wienke et al.* since the presented dataset was obtained from the same paradigm in [4]. *Wienke et al.* defined MW as an individual mental process in which thoughts drift away from the relevant task into an internal train of thought that occurs potentially during neuronal sleep-like activity moments. Concerning the N2pc, they examined how attentional selection varies throughout MEG-recorded MW periods in a pop-out visual search task (see section 4.1.2 for a detailed explanation of the visual paradigm). Randomly interspersed focus level questions were used to measure MW by self-report. They found that the N2pc, which measures visual attentional selection, increased neural activity as performance declined during MW, which may have been a compensatory mechanism for mental distractions [4].

4 Method

The dataset used in this thesis was acquired from the same experimental paradigm used in the experiment of *Wienke et al.* that utilized MEG recordings [4]. However, the dataset for this thesis involved different participants, and the MEG recordings were collected simultaneously with EEG recordings. This section begins by describing how the associated study obtained the data, followed by the description of the dataset. Then, the conventional method to extract the ERP/ERF component reflects the attentional shifts. The decoding algorithm will be explained in detail involving the classification process involving k -fold cross-validation and SVM classifier. The classification performance will be reported as the decoding accuracy and other metric evaluations. At last, statistical significance analyses were conducted to confirm the reliability of the results.

4.1 Dataset

Despite data recording was not part of this master project, detailed information about the experimental setup is provided in the following section because it is essential to understand how the datasets were assembled.

4.1.1 Participants and Recordings

The recordings involved 16 healthy participants with normal or corrected-to-normal vision who were different from the participants in the study of *Wienke et al.*. Three of them were excluded because of unmatched log files (due to some technical issues during recording). The recording process took place at the Department of Neurology, Otto-von-Guericke University of Magdeburg, and was approved by the local ethics committee. All participants received written informed consent and were paid.

Participants were equipped with metal-free clothing and seated in a dimmed, magnetically shielded recording chamber in which EEG and MEG data were simultaneously recorded while undergoing the experiment. The EEG activity was recorded at 29 Ag/AgCl electrodes (Fz, Cz, Pz, Oz, Iz, Fp1, Fp2, F3, F4, F7, F8, T7, T8, C3, C4, P3, P4, O9, O10, P7, P8, FC1, FC2, CP1, CP2, PO3, PO4, PO7, PO8), according to the extended 10-20 system and referenced against the right mastoid. The electrode impedance was maintained to less than $5k\Omega$. The MEG was recorded using a whole-head Elekta Neuromag TRIUX MEG system (Elekta Oy, Helsinki, Finland) with 102 magnetometers and 204 planar gradiometers. Both recordings were performed in a sitting position, and the sampling rate was set to 2000 Hz during recording. In addition, the eye movements were detected using horizontal and vertical electrooculogram (EOG).

Since the raw EEG and MEG signals are usually noisy, a standard step was implemented in

the Neuromag software using the Maxwell filter method (signal-space separation) to suppress interference sources located far away from the sensors [68]. In other words, this method separates environmental artifacts produced by nearby sources or external interference.

4.1.2 Experimental Paradigm

A visual stimulation paradigm was shown onto a screen 100cm in front of the participants. Responses were provided with the left and right hands via a MEG compatible LUMItouch response system (Photon Control Inc., Burnaby, BC, Canada). Through it, participants were presented with a series of stimulus arrays. Each consisted of 18 gratings in a circular shape divided into two blocks of 9 gratings left and right below the fixation cross (see Fig. 4.1). The grating patterns are shown in 3 colors: red or green as the target and blue as the distractor, with two matching background grey stripes on each colored circle. The target gratings could be tilted left or right from the vertical axis, while the non-target and distractor gratings varied randomly.

The experiment consists of twenty trials of familiarization, then 12 blocks with 100 trials each. At the beginning of each block, participants were asked to attend their attention either to the red or green targets and respond by pressing a button in which direction the gratings orientate (left or right). Target color assignment was alternated blockwise, i.e., in blocks where red gratings were the target, the green gratings served as non-target, which needed to be ignored and vice versa. The location of the non-target was mirrored to the opposite side of the target, which could appear at each of the 18 locations, keeping the equal distances to the fixation cross. Participants received a pseudorandom experience sampling probe in 20% of all trials during the experiment to score their attentional focus on a scale of 1 (thoughts were anywhere else) to 5 (thoughts were entirely at the task), reflecting their three mental states (OFF 1 and 2, MID: 3, ON 4 and 5). Responses were given with all five fingers of their left hands.

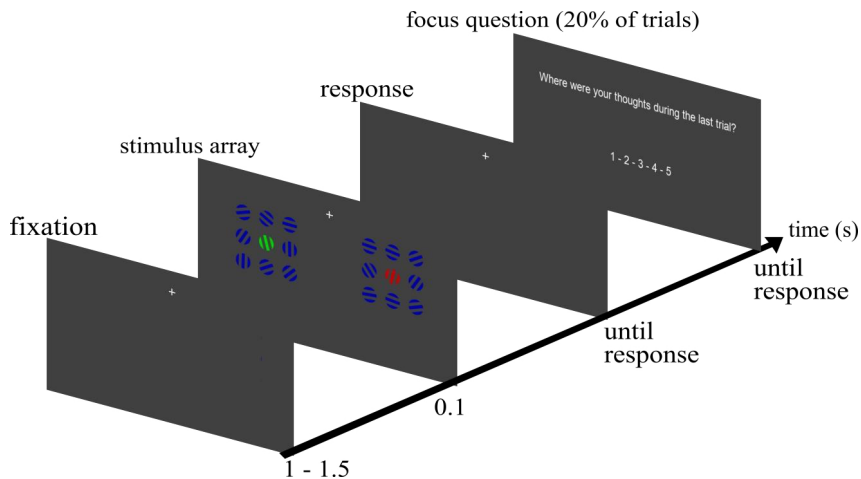


Figure 4.1: Single-trial paradigm with a focus question [4].

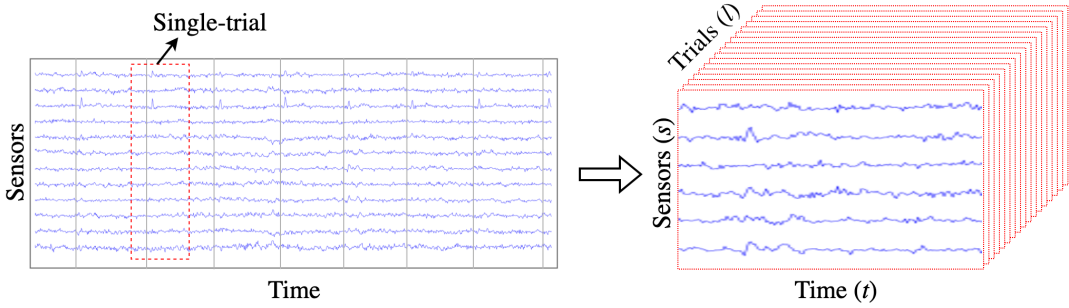


Figure 4.2: Continuous recording into epochs (the signal figure was taken from [69]).

4.1.3 Dataset Preparation

All recorded information, such as the raw EEG and MEG data, electrode names, participant responses, and so on, were stored as log files. The raw EEG and MEG data were continuous signals and sampled at $500Hz$. They were segmented out into epochs parallel with the other log files, corresponding to the sent trigger indices to the recording device, marking the event codes of a single trial where stimulus and response occurred with a total of 1200 trials (see Figure 4.2). The epoch period was designed to start $500ms$ before stimulus onset and last $1500ms$, ending $1000ms$ after stimulus onset. Consequently, the epoching formed a 3-dimensional matrix of a data structure for each participant, i.e., $\mathbf{X}^l \in \mathbb{R}^{s \times t}$, where matrix \mathbf{X} represents the epoched data with the row s (sensors: EEG = 29, MEG = 102) by the column t (sampled time points = 1501) that consist of l trials ($N = 1200$).

Due to uncertainty over whether participants correctly perceived the stimulus, only the correct behavioral responses (corID) were used. The responses were regarded as correct if the behavioral responses aligned with the log files containing the expected responses. Correct responses allowed us to assume that all participants accurately comprehended the visual task. In other words, the attention shifts will be present. The incorrect responses (badID) were retained for the purpose of evaluating the decoding performance.

4.2 Preprocessing

The epoched signals preprocessing was necessary to obtain clean signals for the ERP/ERF analysis (section 4.3) and decoding process (section 4.4). The order of preprocessing was chosen based on a recommendation in a typical ERP experiment made in [13, Appendix], see Figure 4.3. However, several procedures required adjustments for decoding purposes, which will be discussed more below. The EEG and MEG signals tend to be noisy or have DC offsets over time because of their vulnerability to environmental interference and artifacts, such as muscle activity.

Filtering could overcome such unwanted signals as a standard step in signal analysis [70]. All filtering used zero phase-shift IIR filters 4th order (*filtfilt* function in MATLAB® R2016b) and was applied to the epoched EEG and MEG as done in [4]. Given the sampling rate $f_s = 500Hz$, a band-pass filter between 1 and $200Hz$ was sufficient to prevent aliasing, as it is not higher

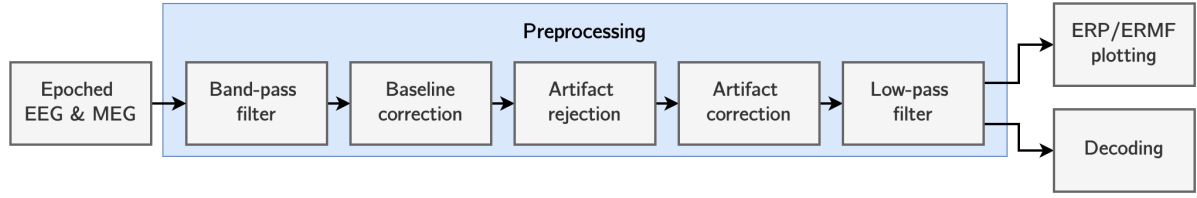


Figure 4.3: Preprocessing block diagram.

than the Nyquist frequency ($f_s/2$) [71] [72, Ch. 3]. The epoched EOG was band-pass filtered between 1 and 30Hz where the presumable muscle activity (i.e., eye movement) was present. A low-pass filter 12.5Hz and downsampling to 50Hz were applied during the decoding to remove redundancies and reduce the complexity of the feature space so the decoder could work faster [65]. In ERP/ERF analysis, a low-pass filter 30Hz was applied to the signals after averaging for visualization purposes.

Each trial of the epoched and filtered signals was baseline corrected to eliminate the DC offsets. The signal power 100ms before the stimulus onset is a reasonable offset estimate, regardless of the noise contamination. By taking the mean of activity within the prestimulus baseline period, most noises will average out, producing an excellent voltage or magnetic field offset estimation. Then, the mean prestimulus from every point in the epoch was subtracted, causing the whole waveform to shift around zero.

In some trials, the artifacts containing irrelevant eye movement and excessive amplitude might cause the epoched signals to be noisy. These artifacts were excluded based on a fixed threshold based on visual inspection on the current dataset: $200\mu V$ for EEG; $3pT$ for MEG (as used in [4]), which the signal values could not surpass. This thesis applied hEOG correction only for ERP/ERF analysis but not decoding since eye movements might increase decoding accuracy. The trials that carry EEG or MEG signals with hEOG-like components were rejected to obtain horizontal eye movement-free signals (artifact correction). They likely contributed to the EEG and MEG signals as the participants needed to pay attention to the left or right presented target. Hence, the artifact correction was useful to visualize cleaned ERP/ERF. Lastly, the temporal interval of the preprocessed data was segmented, beginning at 100 ms before stimulus onset and ending at 800 ms after stimulus onset.

4.3 Spatial Attention Shift

The concept of visual-spatial attention shifts was already explained in the background section 2.2. The corresponding ERP/ERF component, N2pc, indexes the spatial attention of the participants as they paid attention to the target in the visual search task. Given the two recording tools used in this study, the procedure to extract the N2pc was slightly different.

4.3.1 N2pc from ERP

In a typical two-side visual search task (LVF and RVF) analysis using EEG, N2pc can be isolated by collapsing ERP waveforms recorded during LVF and RVF target presentation that was recorded over the left and right hemispheres, i.e., contralateral minus ipsilateral waveforms [2,31]. First, the epochs with LVF and RVF targets were separated and involved only 12 parieto-occipital channels (left cortex: P3, O9, P7, CP1, PO3, PO7; right cortex: P4, O10, P8, CP2, PO4, PO8). The ERP waveforms were then combined to create the contralateral (average of RVF for the left hemisphere and LVF for the right hemisphere) and ipsilateral (average of LVF for the left hemisphere and RVF for the right hemisphere) waveforms. Subtraction of the ipsilateral waveform from the contralateral waveform eliminates bilaterally evoked components and isolates the N2pc [31] [13, Ch. 3]. A paired t-test was performed to reveal significant differences between contralateral and ipsilateral waveforms in each participant, typically found around 200-300ms poststimulus and referred to as N2pc.

4.3.2 N2pc from ERF

The magnetic equivalent of ERP from MEG is ERF. According to previous studies, extracting N2pc analog (mN2pc) from ERF required a slightly different approach from ERP for EEG [7,73,74]. The separated magnetic responses for epochs with LVF and RVF targets were compared using a t-test for each subject. As determined by the t-test, the RVF target response subtraction from LVF target responses removes activity attributed to purely sensory responses [4, 7, 73, 75]. The t-values were utilized to opt specific channels by measuring the maximum positive and maximum negative in each hemisphere, generating four specific channels: efflux and influx channels in both hemispheres. The channels were chosen from the occipitotemporal region of interest (ROI) within 200–300ms poststimulus time window, where the N2pc was expected to be significant [7, 75]. To this end, the N2pc emerges as an influx–efflux difference field in the left hemisphere and as an efflux–influx difference field in the right hemisphere [73] for LVF and RVF targets independently in each hemisphere, then taking the average of these ERFs across trials. These averaged ERF were then used to extract the N2pc in the grand average by subtracting the averaged RVF signals from LVF signals accordingly for both hemispheres from all participants [4].

4.4 Decoding Algorithm

This study demonstrated an offline classification method for decoding visual-spatial attention shifts (N2pc) from the collected EEG and MEG datasets (\mathbf{X}_{EEG} and \mathbf{X}_{MEG}). These data matrices hold spatio-temporal properties $\mathbf{X}^l \in \mathbb{R}^{s \times t}$ for each trial l : s is the number of channels and t is the number of sampled time points, as described in section 4.1.3. All parieto-occipital channels were used in the EEG decoding, as the N2pc was known to be maximum in these areas [31], which was also implemented in [64, 65]. While in the MEG decoding, the occipito-temporal channels were used where the N2pc source activity originates from these regions according to previous findings [7, 75]. The epoched and preprocessed signals played the role of the predictors \mathbf{X} to classify the side where the target appeared in the visual field by discriminating

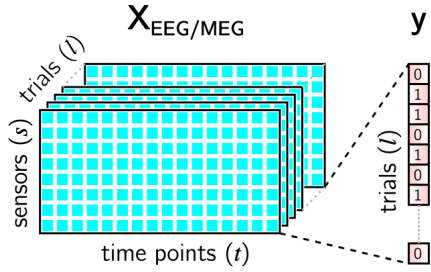


Figure 4.4: The structure of predictor and labels.

between the LVF and RVF. The information about where the target actually appeared served as the label \mathbf{y} with two classes, i.e., 0 for target shown in the LVF and 1 for target shown in the RVF. Figure 4.4 showed the structure of predictors and labels and how each class was assigned to the trials.

4.4.1 SVM Classifier

It was suggested by *Lotte* that SVM as a classifier has shown robust decoding performance and is not dependent on the feature space's complexity, which is beneficial for high-dimensional brain data [17, 52, 76]. Given training vectors $(\mathbf{x}_i, \mathbf{y}_i)$, $i = 1, \dots, n$ where $\mathbf{x}_i \in \mathbb{R}^d$ is a d -vector of predictors and $\mathbf{y}_i \in \{-1, +1\}$ is its binary class, the SVM tries to map the \mathbf{x} into a high dimensional feature space and find a decision boundary (hyperplane) [77, Ch. 5] [78] that is defined by

$$h(\mathbf{x}_i) = \text{sign}\{\mathbf{x}^\top \beta + \beta_0\} = \begin{cases} +1, & \text{if } \mathbf{x}^\top \beta + \beta_0 \geq 0 \\ -1, & \text{else,} \end{cases} \quad (4.1)$$

[79, Ch. 3] [46, Ch. 12] where the *sign* function returns class +1 for the point above or on the hyperplane, whereas class -1 for the point below the hyperplane (see Figure 4.5 for illustration). Assuming that at least one hyperplane can separate the training data, the $h(\mathbf{x})$ function is equivalent to $\mathbf{y}_i h(\mathbf{x}_i) > 0 \forall i$ [46, Ch. 12]. As a result, more hyperplanes may exist to separate other training data accurately. The optimization problem of finding the hyperplane with the maximum margin between classes can be expressed as follows:

$$\min_{\beta, \beta_0} \frac{1}{2} \|\beta\|^2 + C \sum_{i=1}^N \xi_i \quad (4.2)$$

$$\text{subject to } \xi_i \geq 0, \quad y_i(\mathbf{x}_i^\top \beta + \beta_0) \geq 1 - \xi_i \quad \forall i \quad (4.3)$$

[79, Ch. 3] [46, Ch. 12]. The cost parameter C governs the trade-off between the slack variable penalty ξ and the margin distance M . This study used the C estimation for regularization parameter as suggested by *T. Joachim* [80, Ch. 11] [79, Ch. 3]:

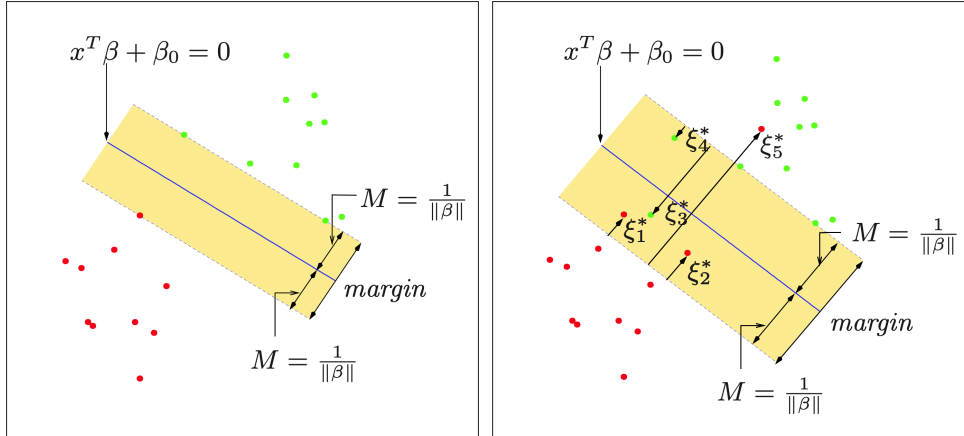


Figure 4.5: Hyperplane in Support Vector Classifier

Separable data (left) and non-separable data (right). The decision boundary is denoted with the solid line, and the maximal margin is denoted with broken lines [46, Ch. 12].

$$C = n / \left(\sum_{i=1}^n \mathbf{x}_i \cdot \mathbf{x}_i \right) \quad (4.4)$$

The *fitcsvm* function in MATLAB® R2016b was used for the SVM classifier training. Some input arguments were added, the kernel function was set into default as linear since this is two-class learning, and the box constraint was defined using the C parameter 4.4. These processes were run in k -fold cross-validation, where the given datasets were divided into training and testing subsets for k iterations (see Section 4.4.2 for further explanation).

Figure 4.6 shows that some trials were preselected for SVM training then used for the classifier input. Only the corID data was involved for training since it reflects the correct visual task interpretation of the participants. Given the two-class dataset for training, the distribution of the classes was initially balanced (50:50). However, the number of trials was reduced due to preprocessing, leaving the classes imbalanced. Before the training, a non-heuristic method randomized undersampling was performed on each participant independently to ensure that the classification results were not biased. First, the majority and minority classes were established based on class size. The majority class was then randomly cut off to achieve equal instances as the minority class.

Let $(\mathbf{X}_{train_i}, \mathbf{y}_{train_i})$ for $i = 1, \dots, l$ where every training data $\mathbf{X}_{train_i} \in \mathbb{R}^{s \times t}$ was paired to its corresponding class $\mathbf{y}_{train_i} \in \{0, 1\}$. Due to 50Hz resampling, the sampled time points $t = 1501$ can be written as $d = 41$, corresponding to the time interval of 0 to 800ms. Adapting the feature selection from *Blankertz et al.*, the feature was considered to represent every sampled time point t in each channel s within trial i , i.e., spatio-temporal features [59]. It is essential to extract the spatio-temporal features by concatenating all columns of \mathbf{X}_{train} into $\mathbf{x}_{train} \in \mathbb{R}^F$, where $F = s * d$. As a result, the dimension of the feature vector of EEG was 574 (14 parieto-occipital channels * 41 sampled time points), and MEG was 2050 (50 occipito-temporal channels * 41

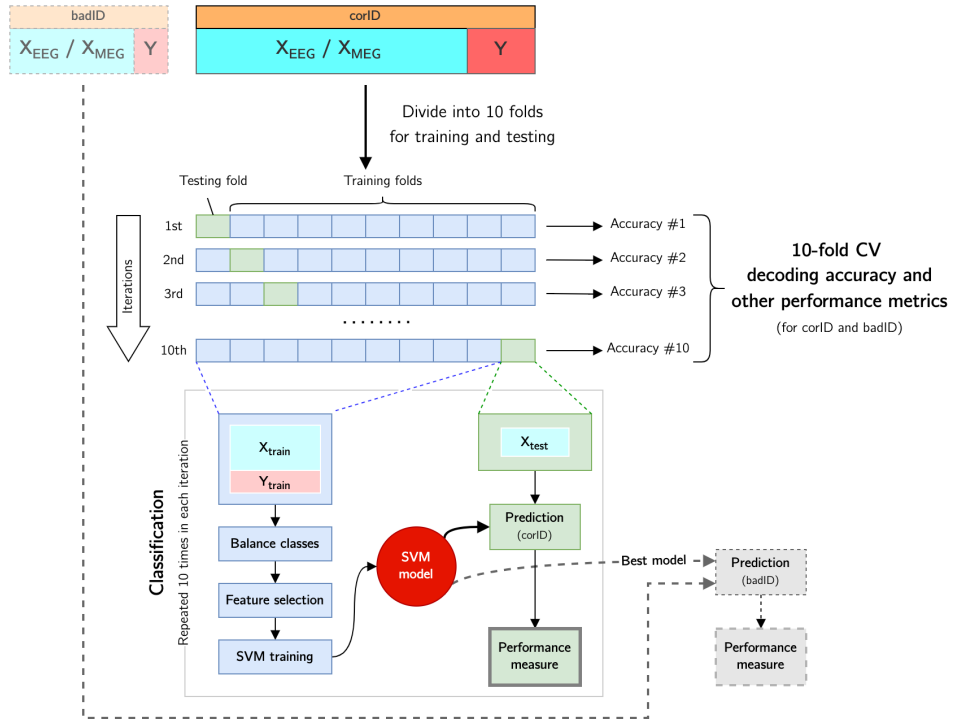


Figure 4.6: Decoding Algorithm Pipeline.

sampled time points). Hence, the input predictor for training can be denoted as $\mathbf{X}_{train} \in \mathbb{R}^{l \times F}$, where every row is a single-trial.

The trained output was the SVM model, which was used to classify some preselected $\mathbf{X}_{test} \in \mathbb{R}^{l \times F}$ using predict function. The classification resulted in predicted classes according to the trained SVM model. How well the classifier performed in terms of decoding accuracy was measured from all iterations averaged (see Section 4.4.5), and this was done for each participant. In addition, how the developed decoder dealt with the badIDs was also evaluated. See the decoding pipeline using 10-fold cross-validation in Figure 4.6.

4.4.2 K-Fold Cross-Validation

Cross-validation estimated the performance of the decoding algorithm in conducting predictions on limited datasets that have not been trained on. The parameter k denotes the number of folds used to partition the provided dataset (\mathbf{X}_{EEG} and \mathbf{X}_{MEG}) in each iteration. In this thesis, $k=10$ was chosen as it is a commonly used value in the cross-validation approach [81, Ch. 5]. The dataset partition was done by dividing the dataset into k equally sized folds, consisting of some trials assigned for training (consisting of $k-1$ subsets) and the remaining for testing. In each fold, the chosen trials can only be trained and tested one time in that particular fold, then a different set of trials in the other iterations. The classification was done 10 times to acquire an average performance during each iteration. The 10-fold cross-validation decoding accuracy was determined from overall average performance throughout all iterations.

4.4.3 Spatio-temporal Filters Estimation for Classification

To maximize the spatial and temporal information of EEG and MEG, SNR must be enhanced using spatial filters. Correspondingly, the classification of visual-spatial attention shifts may have higher accuracy. This analysis used the CCA to build a spatial filter, which was adapted and closely connected to the CCA approach used in [55, 64–66, 82], which estimates spatial-temporal filters canonical components of the same training data assigned to the classifier.

In principle, CCA determines linear transformations of two datasets of variables (\mathbf{X} and \mathbf{Y}) with any underlying similarities, which maximizes the transformed datasets' correlations, namely $\mathbf{u}^T \mathbf{X}$ and $\mathbf{v}^T \mathbf{Y}$,

$$(\mathbf{u}', \mathbf{v}') = \underset{\mathbf{u}, \mathbf{v}}{\operatorname{argmax}} \operatorname{corr}(\mathbf{u}^\top \mathbf{X}, \mathbf{v}^\top \mathbf{Y}) \quad (4.5)$$

where \mathbf{u}' and \mathbf{v}' are the resulting canonical variables. As mentioned above, a matrix that represents EEG and MEG can be written as $\mathbf{X}_{\text{train}} \in \mathbb{R}^{s \times d}$ is the preprocessed signals resulted in $d = 41$ of time points, involving $s = 14$ channels (EEG) and $s = 50$ channels (MEG). Target stimuli occurred in either LVF or RVF labeled with 0 or 1, respectively. For the simplicity of interpreting the labels, $\mathbf{y}_i \in \{0, 1\}$ is equivalent to $\mathbf{y}_i \in \{-1, +1\}$.

For each stimulus sequence at which side the target appeared, a series of reference functions \mathbf{Y}^f is modeled, i.e., concatenation of identity matrices $\mathbf{I}_d \in \mathbb{R}^{41 \times 41}$, weighted with the associated labels \mathbf{y}_i . Consequently, $-\mathbf{I}\mathbf{y}_i$ represents that the participant focused on a target stimulus presented on the LVF, and $\mathbf{I}\mathbf{y}_i$ represents that the participant focused on a target stimulus presented on the RVF. \mathbf{Y}^f can be called a weighting matrix by the matrix multiplication

$$\bar{\mathbf{X}} = \mathbf{Y}^{fT} \mathbf{X}, \quad (4.6)$$

which subtracts the sum over stimuli in \mathbf{X} representing RVF stimulation from the sum over stimuli in \mathbf{X} representing LVF stimulation, so that $\bar{\mathbf{X}} \in \mathbb{R}^{s \times d}$ represents the discrepancy between the combined brain data and following left presentations and right presentations. This is usually achieved when identifying the N2pc component, essentially by investigating the difference of waves [1, 7, 64]. However, the aim is to build an optimal spatial filter from the training dataset. Thus, CCA is applied with the equation 4.5 to \mathbf{X} and \mathbf{Y}^f using the MATLAB® function *canoncorr* of the Statistics and Machine Learning Toolbox™.

The MEG data of all trials are concatenated to \mathbf{X} , and the relevant reference functions for the known target position are concatenated to \mathbf{Y} . Coefficients of \mathbf{u} can be considered as a spatial filter that combines the channels with substitute channels \mathbf{u}' while coefficients in \mathbf{v} modify the waveform \mathbf{v}' , which corresponds to the substitute channels maximally. Once the resulting canonical coefficients \mathbf{u}' and \mathbf{v}' are calculated, they can be applied as a spatial filter on new data. In this particular case, the spatial filter was applied to training data $\mathbf{X}_{\text{train}}$ and testing data \mathbf{X}_{test} before classification.

4.4.4 N-Combined Trial Sets

A slightly different procedure was carried out by generating n -combined trial sets for training and testing. The step was done to increase the SNR and decodability of the attention shifts ($N2pc$) by means of averaging some number of ERP trials [9]. Assuming the number of classes in \mathbf{X}_{train} was balanced, the \mathbf{X}_{train} was grouped based on the classes, i.e., the first half belonged to the first class ($\mathbf{y}_i = 0$), and the second half belonged to the second class ($\mathbf{y}_i = 1$). The number of combined trials n ranged from 1 to 10, which the first n being a single trial, and there is no need to create a combined trial set when $n = 1$. During the combined trial set creation, n randomly chosen trials of \mathbf{X}_{train} were averaged. The averaged \mathbf{X}_{train} was then rearranged as a new trial. This process was repeated for every trial in each class group, which became the combined trial set.

4.4.5 Evaluation Metrics

All of these procedures were repeated in each iteration of the cross-validation. Alternately, 90% of the data were for training, and 10% were for testing until all subsets had been tested once [63]. The predicted results were finally evaluated by calculating their accuracy for each subject, which was addressed as decoding accuracy. Accuracy could be conveniently estimated by calculating the number of correct predictions by the total number of predictions [83]. Thus, the classifier's prediction results can be formulated with a confusion matrix below.

Table 4.1: Confusion Matrix of Binary Classification [84]

		Actual	
		1	0
Predicted	1	True Positive (TP)	False Positive (FP)
	0	False Negative (FN)	True Negative (TN)

The positive and negative terms refer to the predictions of the classifier. In our case, the negative corresponds to the target presented to the left (class 0), and the positive corresponds to the target presented to the right (class 1). Terms true and false indicate whether that prediction corresponds to our observations (predefined label).

$$Accuracy = \frac{TP + TN}{TP + TN + FP + FN} \quad (4.7)$$

Since both conditions (1 and 0) represented each class, the probability of class-relevant trials that were correctly predicted for each class, called a recall, can be predicted. That makes the recall for each class is equivalent with:

- *Sensitivity* or true positive rate (TPR), which described what percentage of class 1 were correctly identified. Thus,

$$TPR \text{ of class 1} = \frac{TP}{TP + FN} \quad (4.8)$$

- Furthermore, for class 0, on the other hand, it is called *specificity* or true negative rate (TNR), meaning that this measure is precisely the opposite of *sensitivity*. It can also be referred as the TPR of class 0. This is valid as long as the data that has been predicted was binary. Therefore,

$$TPR \text{ of class } 0 = \frac{TN}{TN + FP} \quad (4.9)$$

4.5 Analysis of the Decodability

The results were analyzed using MATLAB® R2016b and JASP software (Version 0.16) [85]. We tested a classification of attentional shifts by evaluating the decoding performance results compared to several factors.

4.5.1 Significance Test for Decoding

A permutation test was used to evaluate the significance of the decoder by randomly permuting the labels across trials 1000 times, then performing the classification. This permutation test assured that the corresponding classes to their respective trials were ruined while keeping the trial distributions unaltered [86]. The unpermuted decoding accuracy results were compared against the permuted performance and we determined the 95% confidence intervals of the permutation test. Given the work of *Pereira et al.* [87], the performance of the developed decoder is dependable (non-random) and statistically significant if the decoding accuracies are above the chance level and outside the confidence intervals [88,89]. Hence, our hypotheses were as follows:

H_0 : Decoding performance values are within the 95% confidence intervals of the permutation test distributions, indicating that the attentional shifts are not reliable enough to be decoded.

H_1 : Decoding performance values are outside the 95% confidence intervals of the permutation test distributions, indicating that the attentional shifts are reliable enough to be decoded.

Paired two-sided Wilcoxon signed-rank was used to test the significance between two distributions of decoding accuracy, and the test statistic was denoted by W . It should be noted that the decoding performances of all 13 participants were affected by several aspects, including the recording techniques (EEG and MEG), the role of the spatial filter (with and without), and the number of combined-trial sets ($n = [1..10]$). Using the repeated measures ANOVA followed by post hoc with Bonferroni correction [90], further statistical analyses were performed to examine the influence of these parameters on decoding accuracy.

4.5.2 Decoding Performance Towards Incorrect Trials

The decoding accuracy results were essentially a measure of how robust the classifier model predicted the testing set. Nevertheless, the testing set was determined from the trials where

participants responded correctly or corID. An additional investigation was done using the trained classifier model to predict a new testing set that indicated the participants responded incorrectly or badID. ANOVA was employed to see any significance between the badID and corID, recording techniques, STF involvement, and n -combined trials.

4.5.3 Decoding Performance Comparison with a Published Dataset

As stated above, this thesis employed the same visual task paradigm and MEG recording setup as Wienke et al. used. The published MEG dataset from the study could be used as a secondary dataset to validate the developed decoding algorithm. With the permission of the authors, we reanalyzed their data with our approach. Hence, the decoding performance of the published MEG dataset was compared to the current MEG dataset. The comparison was based on mean decoding accuracy in each combined-trial set ($n = [1..10]$).

4.5.4 Focus Rate and Decoding Accuracy Correlations

Participants assessed their mental state in the 20% of randomly selected trials, either being focused on the task (ON), in between focused and mind-wandering (MID), or mind-wandering (OFF). The number of these trials vary between participants. Only the corIDs from these focus rate trials were involved, increasing the probability that attention shifts were indeed successfully performed. The ratio of trials in each participant's ON and OFF state was correlated with their respective decoding accuracy to investigate the possible relationship between them. Pearson's correlation coefficient r was used to evaluate any potential correlation between the focus level ratio and decoding performance.

5 Results

5.1 Decoding Performance of Single-Trial

The EEG and MEG decoding performances were obtained using our decoding approach, i.e., the 10-fold cross-validation of the linear SVM. From the results of the permutation test, the empirically estimated guessing level was averaged over subjects ($i=13$), the usage of STF (with and without), and combined-trial sets ($n = [1..10]$). It was 50.89% in EEG and 49.31% in MEG recordings, with their respective upper 95% confidence interval of 56.1% and 58.37%.

For the single-trial ($n = 1$) EEG, the decoding accuracy of 12 out of 13 participants exceeds the chance level and outside the 95% CI of the permutation test ($\mu = 67.927\%$, $\sigma = 7.692\%$, $max = 81.101\%$, see Figure 5.1a), which was statistically significant ($W = 91$, $p < 0.001$) as reported by the Wilcoxon signed-rank test. In comparison, the decoding accuracy distributions in single-trial MEG are higher than the chance level and outside the 95% CI of the permutation test ($\mu = 68.895\%$, $\sigma = 8.4\%$, $max = 81.154\%$, see Figure 5.1b), which was also statistically significant ($W = 91$, $p < 0.001$). Thus, there was sufficient evidence to reject the null hypothesis (H_0), indicating that visual-spatial attention shifts were reliable enough to be decoded at the single-trial level. Even though the decoding accuracy distributions within participants between EEG and MEG at the single-trial level appeared to be non-significant ($W = 40$, $p < 0.735$).

Aside from decoding accuracy, the TPRs of each class were displayed in Figures 5.1a and 5.1b, which defined the performance of the class-relevant trials. The TPR of class 0 (green dash) indicated how accurately visual-spatial attention shifts from LVF trials were decoded. The TPR of class 1 (pink dash) indicated how accurately visual-spatial attention shifts from RVF trials were decoded. In the single-trial EEG, the TPRs of both classes were not statistically significant ($p = 0.08$; "0" : $\mu = 68.846\%$, $\sigma = 7.71\%$; "1" : $\mu = 67.601\%$, $\sigma = 8.131\%$). In the single-trial MEG, the TPRs of both classes were not statistically significant ($p = 0.455$; "0" : $\mu = 69.48\%$, $\sigma = 9.395\%$; "1" : $\mu = 68.352\%$, $\sigma = 8.001\%$). TPRs of both classes remained not statistically significant even when STF was applied on both recording techniques and throughout different n-combined trials.

5.2 Decoding Performance in Different Conditions

The statistical analyses have the potential to reveal a recording technique (EEG and MEG) \times STF (with and without) \times the number of combined-trial sets ($n = [1..10]$) interaction on decoding accuracy. The result showed no significant difference in recording techniques ($F(1, 12) = 0.164$, $p = 0.693$). Figure 5.2 depicts the mean decoding accuracy performance in which the EEG (blue bar) and MEG (orange bar) appeared about the same not only in the

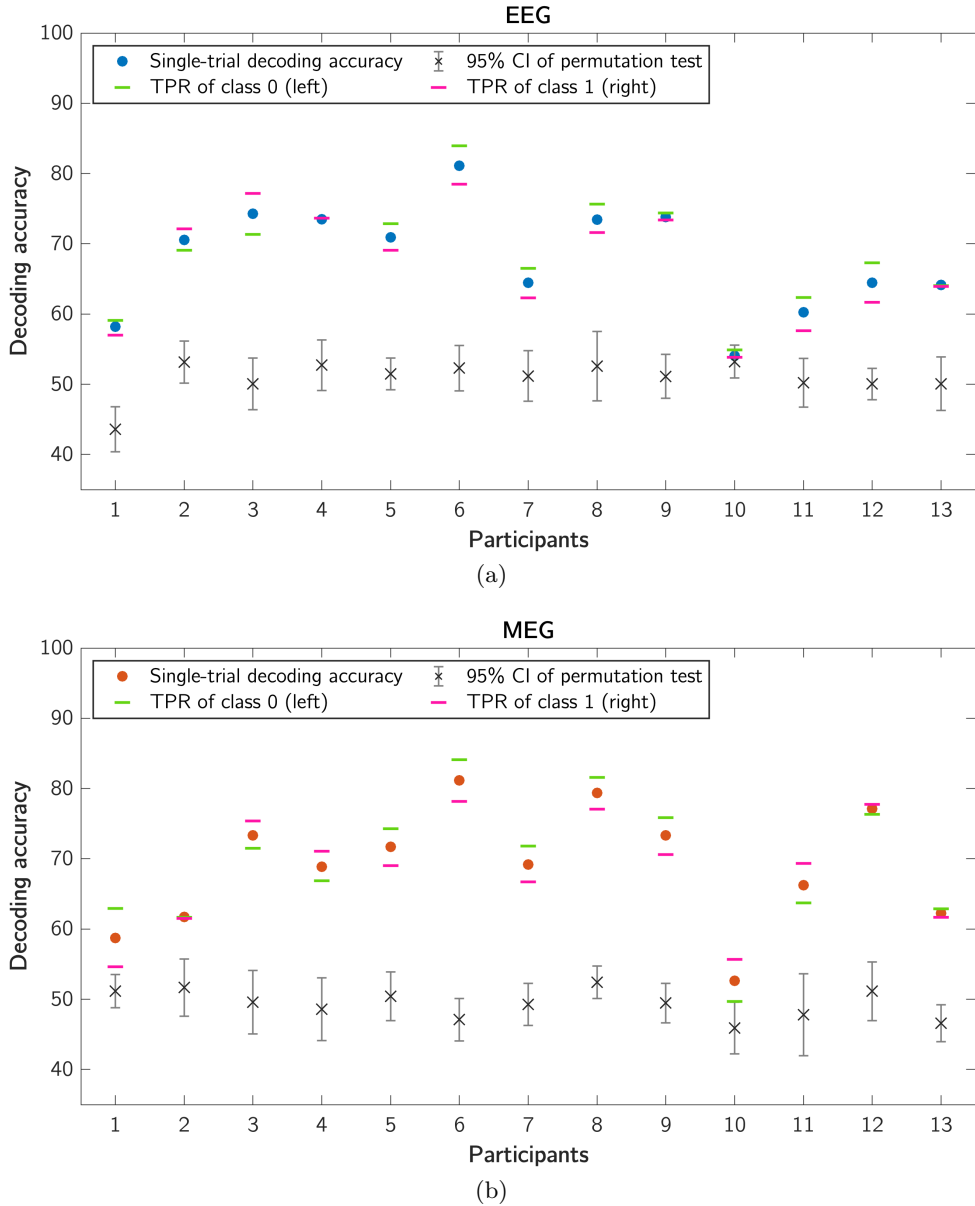


Figure 5.1: Decoding Performance of 13 Participants in Single-Trial Level.

- a) The decoding accuracies in single-trial EEG (blue dot) were accompanied by the TPRs for class 0 (green dash) and class 1 (pink dash), which are primarily outside the 95% confidence interval for the permutation test (grey whisker with an x). b) The decoding accuracies in single-trial MEG (orange dot) with the same properties as already explained.

single-trial but also throughout combined-trial sets ($n = 2 : 10$), with the mean decoding accuracy in MEG being slightly higher than in EEG. All values of mean decoding accuracy (corID) were summarized in Table 5.1.

On the other hand, the use of STF showed a significant effect on decoding accuracy ($F(1, 12) = 58.731, p < 0.001$). The effect of STF was more dominant in EEG over MEG in each combined-trial set. In 5.2, EEG with STF (violet bar) always appears higher than MEG with STF (yellow bar). The significant effects on decoding performance were also shown as the number of trials to be averaged increased for combined-trial sets, i.e., from the single-trial $n = 1$ to $n = 10$.

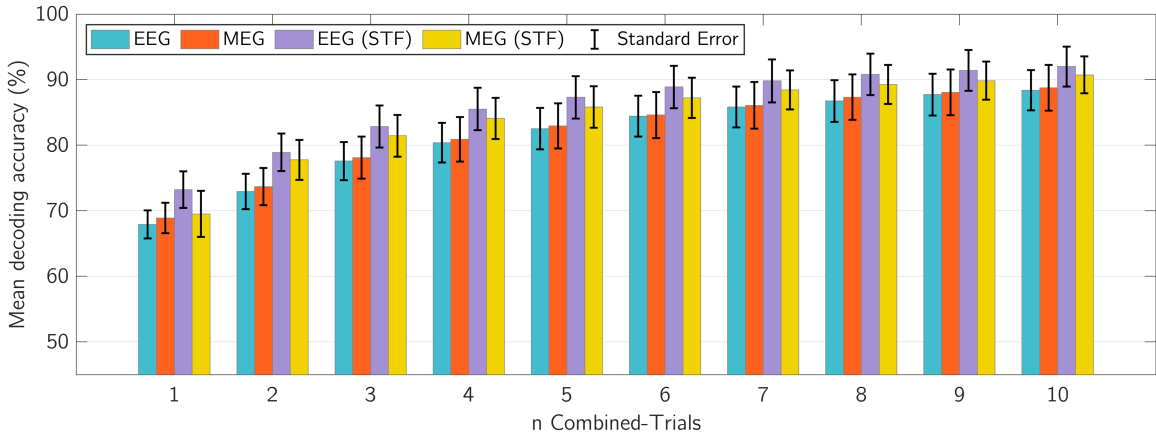


Figure 5.2: Mean Decoding Accuracy of EEG and MEG.

These are the primary findings from the current dataset regarding n-combined trials. Each bar is color-coded and described in the legend.

$(F(9, 108) = 235.012, p < 0.001)$.

The increasing trend of mean decoding accuracy can be observed in Figure 5.3, along with the relative constant mean decoding accuracy of incorrect trials. An interaction of trial conditions (corID and badID) \times recording techniques \times STF \times n-combined trials was done. It revealed that no significant effect was observed in using EEG or MEG ($F(1, 12) = 0.432, p = 0.523$). There were significant effects in applying the STF ($F(1, 12) = 42.108, p < 0.001$), involving n combined-trial sets ($F(9, 108) = 203.434, p < 0.001$), and the corID and badID were statistically significant ($F(1, 12) = 295.176, p < 0.001$).

5.3 Decoding Performance Comparison with a Published Dataset

The datasets were compared based on the mean decoding accuracy across participants and each of the n combined trials. The distributions of the mean decoding accuracies were shown in Figure 5.4. The sign-rank test revealed that there was a difference in mean decoding accuracy between the present (orange bar) and published MEG (cyan bar) datasets ($W = 49, p = 0.027$). However,

Table 5.1: Mean decoding accuracy of EEG and MEG

n	EEG	MEG	EEG (STF)	MEG (STF)
1	67.927	68.895	73.209	69.513
2	72.929	73.673	78.914	77.779
3	77.576	78.105	82.871	81.436
4	80.379	80.893	85.526	84.102
5	82.518	82.932	87.314	85.839
6	84.422	84.608	88.886	87.224
7	85.833	86.081	89.820	88.431
8	86.745	87.325	90.808	89.258
9	87.717	88.056	91.420	89.850
10	88.378	88.764	92.011	90.735

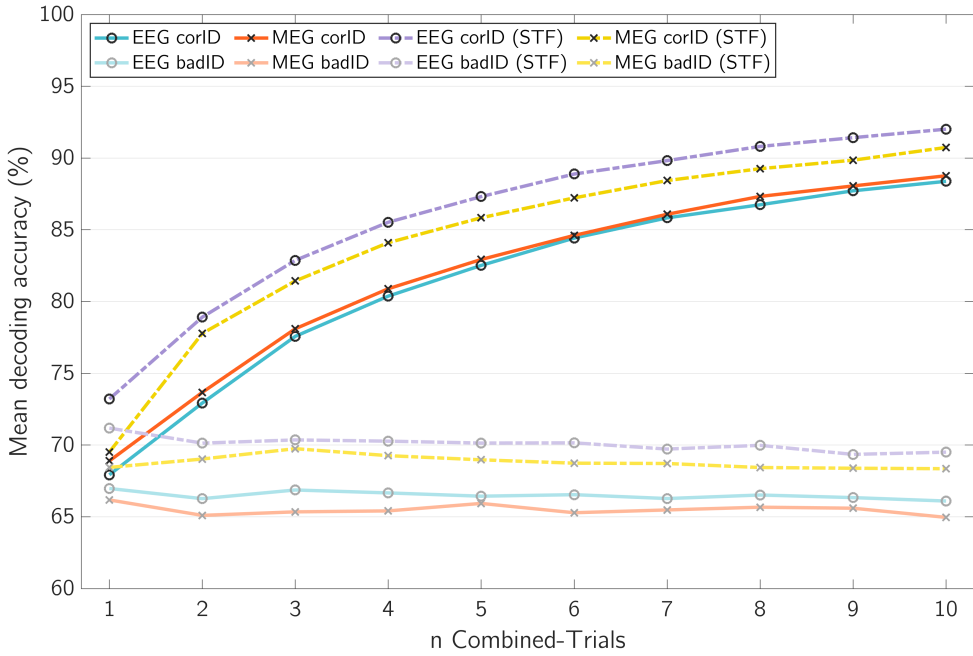


Figure 5.3: Mean Decoding Accuracy Trend of Correct and Incorrect Trials.

The mean decoding accuracies of EEGs and MEGs involving correct trials only (corID) significantly increased from single-trial to the highest n-combined trials, compared to incorrect trials (badID) with relatively over the same accuracy.

visual inspection of the mean decoding accuracy of each n did not show much difference between the present and published MEG datasets. After applying the STF, a significant difference was observed between the present (yellow bar) and published MEG (purple bar) datasets ($W = 0$, $p = 0.002$) with a better performance in the published MEG dataset.

5.4 Focus Level and Decoding Accuracy Correlations

Correlation coefficients were calculated between the decoding accuracies and the focus level ON and OFF ratio when the participants responded correctly. The results showed no significant correlation and were visualized in scatterplot graphs with the linear relationship between two

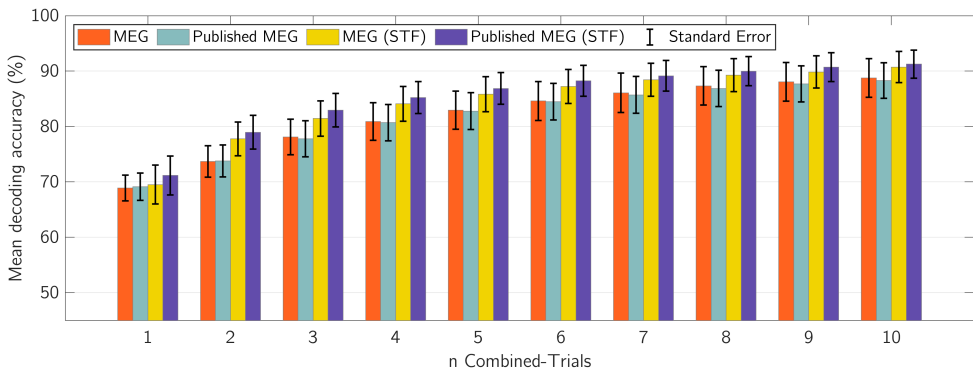


Figure 5.4: Mean Decoding Accuracy of MEG.

A decoding accuracy results comparing the current MEG and published MEG dataset from Wienke et al. Each bar is color-coded and described in the legend.

Table 5.2: Mean decoding accuracy of current and published MEG datasets

n	MEG	$MEG_{published}$	MEG (STF)	$MEG_{published}$ (STF)
1	68.895	69.108	69.513	71.160
2	73.673	73.781	77.779	78.955
3	78.105	77.782	81.436	82.961
4	80.893	80.692	84.102	85.228
5	82.932	82.777	85.839	86.866
6	84.608	84.473	87.224	88.261
7	86.081	85.711	88.431	89.145
8	87.325	86.869	89.258	89.992
9	88.056	87.680	89.850	90.728
10	88.764	88.299	90.735	91.261

variables, Figures 5.5a for correlation between the single-trial decoding accuracy and ON trials ratio (EEG: $r = 0.143$, $p = 0.640$; MEG: $r = 0.331$, $p = 0.269$; EEG (STF): $r = 0.261$, $p = 0.39$; MEG (STF): $r = 0.292$, $p = 0.333$), and 5.5b for correlation between the single-trial decoding accuracy and OFF trials ratio (EEG: $r = 0.395$, $p = 0.181$; MEG: $r = 0.311$, $p = 0.301$; EEG (STF): $r = 0.152$, $p = 0.62$; MEG (STF): $r = 0.408$, $p = 0.167$).

5.5 N2pc Extraction Results

Target and distractors' disambiguation by participants evoked a visual attentional shift indexed by the N2pc component. The collapsed grand average ERP from contralateral (blue line) and ipsilateral (orange-dotted line) waveforms of all participants were illustrated in all parieto-occipital EEG channel pairs in Figure 5.6a. Contralateral minus ipsilateral (thick black line) displayed the N2pc with a more negative peak, which was also highlighted (grey shade) based on the significant difference ($p < 0.05$) between contralateral and ipsilateral waveforms across participants. The N2pc can be seen to occur roughly in between 180ms to 300ms poststimulus on each electrode pair (see Table A.11). According to a visual inspection, N2pc showed prominent negative amplitude in P7-P8 and PO7-PO8 channels.

The grand average ERF of the left and right hemispheres comprised the chosen MEG channels in the occipito-temporal sites that showed maximum efflux and maximum influx collapsed into these grand averages, illustrated in Figure 5.6b. The LVF target waveform is represented with a blue line and the RVF target waveform with an orange-dotted line. The subtraction of RVF from the LVF target waveform revealed the mN2pc (thick black line) as a negative deflection ranging from 184ms to 354ms poststimulus in the left hemisphere and as a positive deflection ranging from 212ms to 330ms in the right hemisphere. The shaded grey area in both hemispheres reflected the temporal significances ($p < 0.05$) when the mN2pc occurred.

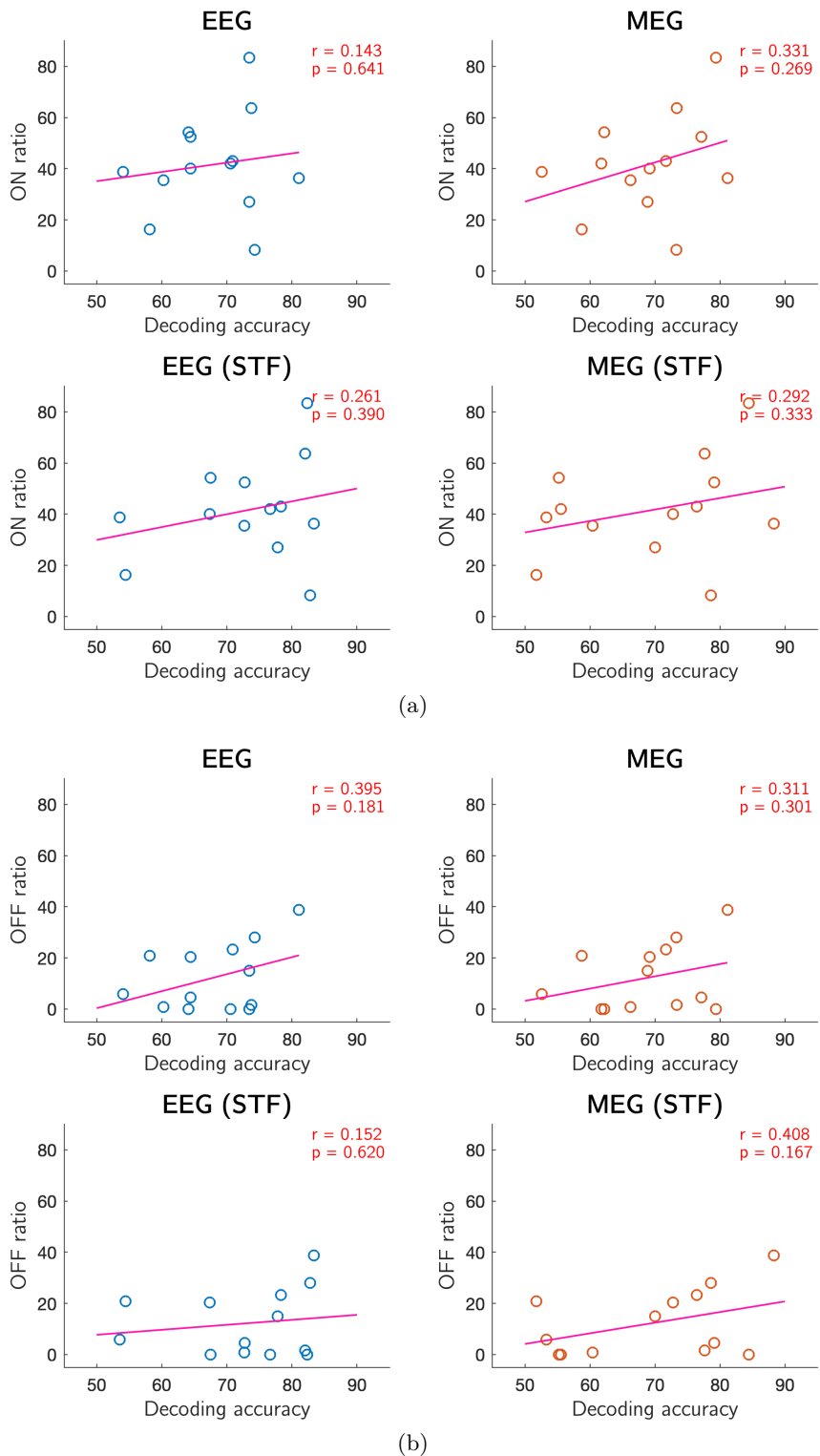


Figure 5.5: Correlation Between Decoding Accuracy and Mental State Ratings

- a) The correlation results from single-trial decoding accuracies against the ratio of ON trials and
- b) the ratio of OFF trials

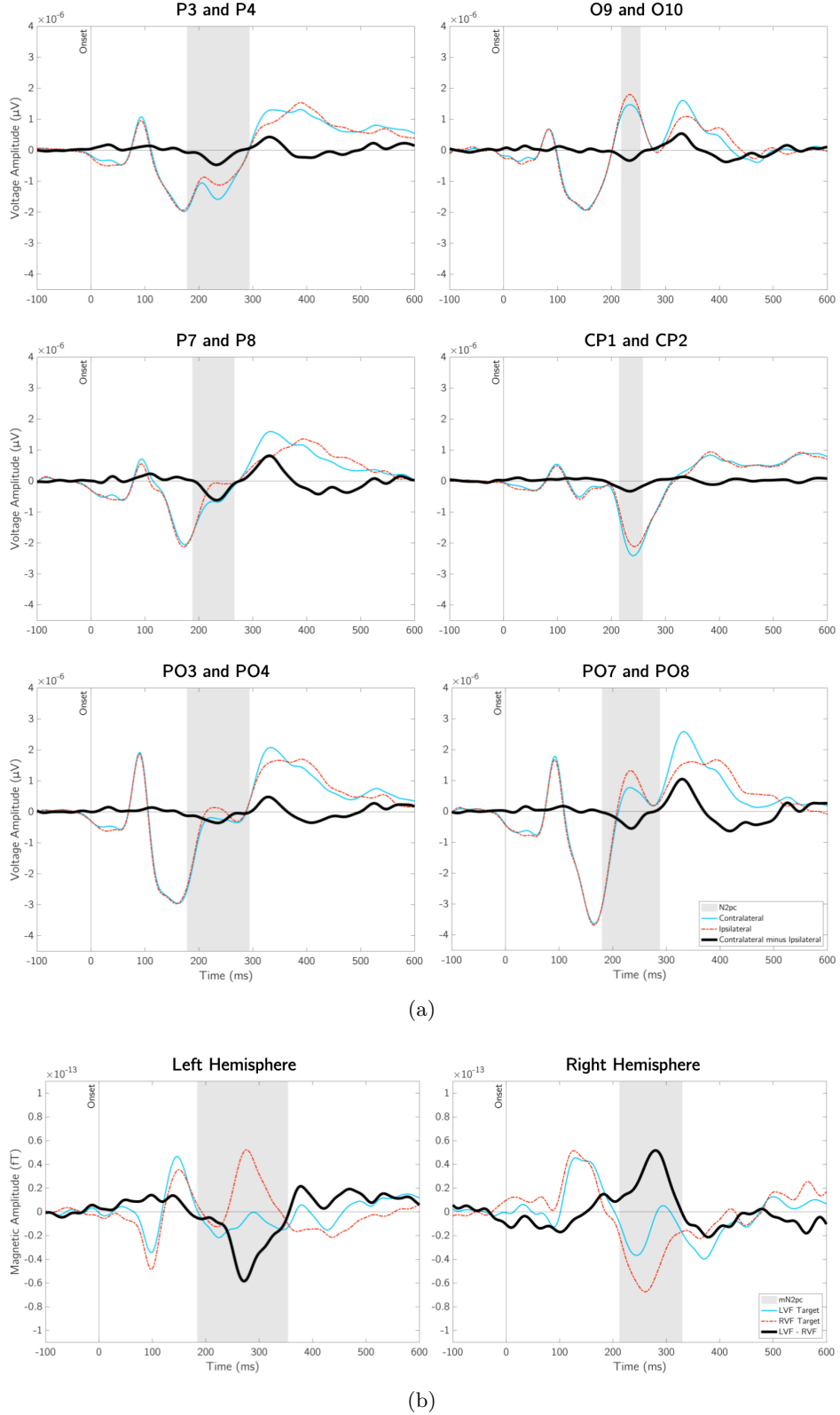


Figure 5.6: Grand Average of ERP and ERF.

a) Contralateral and ipsilateral waveforms for each EEG channel pair revealed N2pc activity in the grand average ERP at around 180ms to 300ms. b) The grand average LVF and RVF target waveform on the left and right hemispheres from the combination of efflux and influx channels showing opposite polarity mN2pc at around 180ms to 350ms.

6 Discussion

Numerous EEG and MEG studies have used the N2pc component in their visual attentional experiment. It offers a precise temporal neural marker that could track relevant target stimuli discriminated against other non-relevant distractors within the LVF or RVF in a visual task [3, 7, 31]. In the present study, the decodability of visual-spatial attention shifts or N2pc was being investigated from EEG and MEG signals by means of an SVM classifier.

6.1 Outcome

The utilization of EEG and MEG recordings in this study was not meant to be combined. Instead, the offline classification performances were observed between both. The first and principal observation was the ERP and ERF decoding performance at the single-trial level ($n = 1$) involving the corID. It showed most individual decoding accuracies outperformed the permutation test and the chance level, which confirmed the hypothesis (see Section 4.5.1). From Table A.1, we can see the mean decoding accuracy was slightly higher in MEG than EEG, but they were not significantly different, and the decoding accuracy within participants did not indicate that MEG was overperforming EEG. Some of the individual decoding accuracy in EEG was higher than in the MEG.

After STF was applied, the mean performance was higher in EEG. This indicates that the application of STF enhanced the decoding accuracy across participants, with decoding accuracies in EEG being higher than in the MEG. Such performance was expected to be caused by STF since it has been known that a CCA-based spatial filter improves the SNR of the filtered signal [57]. The study of *Spüler et al.* performed STF based on CCA for their ERP classification. The CCA spatial filtering in EEG datasets provided consistent high accuracy results compared to other spatial filters [56]. The spatial filtering based on CCA was previously also used in [55, 64–66, 82]. They used CCA to approximate spatial filters and canonical components, which was adapted in this study for the single-trial and every n -combined trial set.

In the present study, adding the number of ERP/ERF trials to create the combined trial set was adapted from the study of *Awni et al.*. Their finding achieved almost 90% accuracy in one of the participants with only three trial combinations ($n = 3$) [9]. While one of our participants reached a slightly higher decoding accuracy at 90.66% from EEG and 94.69% from MEG, with fewer ERP/ERF trials ($n = 2$) and with STF applied. The combined trial set played a role in enhanced decoding accuracy. The more trial combined to create a new set, the more SNR increased. That is why the results showed improved performance as n was increased ($n = [1..10]$). However, there was variability in decoding accuracy from EEG and MEG within participants,

which overperformed each other. According to *Awni et al.*, this variability is presumably due to the degree of familiarity of the N2pc response by the classifier [9]. Therefore, it is reasonable to conclude that visual-spatial attention shifts played a role in decoding performance.

While all the decoding performances results were generated from classification involving corID trials, another additional aspect was investigated to predict unseen badID trials using the trained SVM model. The badID essentially represented the behavioral response of the participants that were not successfully distinguishing the target in the visual paradigm. It was assumed that covert shifts might still occur even when the participants responded incorrectly. However, the results deduced that there might be a minor mistake in the decoding algorithm to process the badID trials. As demonstrated in previous results, the decoding accuracy should have increased as the number of combined trials increased. Instead, the decoding performance of badID was relatively the same over 70% accuracy as n increased.

The probability of the classifier that predicted each class correctly was considered the decoding accuracy of class-relevant trials (TPR of class 0 and class 1). The results showed that both TPRs were similar in all conditions (different recording techniques, STF involvement, different number of combined trials set), implying that the decoder is not biased to one of the classes. This was expected since the size of the class in each participant was balanced before the training with a randomized undersample.

The presented trials of ON and OFF mental state included only correct trials after erroneous trials exclusion, meaning that the ON and OFF ratio presented in the result was the proper outcome when participants confidently rated if they were focused entirely on the task or MW. However, the Pearson's correlation coefficient between the focus level ratio and obtained decoding accuracies showed a weak correlation and were not statistically significant in all conditions, implying that they are not correlated. It can be assumed that the subjective rating during the visual task did not affect the decoding performance.

In the study of *Wienke et al.*, only MEG was used to collect the data and has not been appropriately used for decoding analysis outside the study [4]. With the authors' permission, a decoding comparison was made between the published MEG dataset and the current MEG dataset. Since both MEG datasets were recorded with the same paradigm, the results showed expected performance with roughly the same mean decoding accuracy. Yet, the statistical result indicated that they were statistically significant ($p = 0.027$). The mean decoding accuracy of both datasets was indeed improved across n -combined trials set but still with relatively the same value. In this case, no significant effect was seen on the data. However, the mean decoding accuracy improved after STF was applied on both datasets. It was also observed that the performance of published MEG was always higher than the current MEG across n -combined trials. In this case, it was reasonable to confirm the significant difference ($p = 0.002$) in the mean performance between the current and published MEG. This is probably because *Wienke et al.* did not record EEG simultaneously. Hence the SNR was more excellent, and the combination of STF enhanced the performance even better.

At this point, the main goal of this thesis has been discussed. Additionally, the N2pc from ERP and ERF analysis was also investigated conventionally (see Method 4.3). In the grand average EEG waveforms, the N2pc was seen more prominent in parieto-occipital EEG channel pairs P7-P8 and PO7-PO8 at roughly around 180-300ms. This is aligned with the common theory that N2pc is commonly elicited near the PO7 and PO8 [31], which some studies sometimes also explored N2pc at P7 and P8 [91, 92], or both [93]. In the grand average MEG waveforms, the mN2pc was seen as opposite-polarity in the left and right hemispheres, elicited at roughly around 180-350ms. Unlike EEG, the grand average of MEG was composed of influx-efflux maxima channel at the occipito-temporal site from each participant [7, 62, 75].

6.2 Limitation and Future Work

This thesis is a preliminary approach to creating a decoding algorithm of attentional shifts component for future BCI paradigm. Therefore, it is crucial to point out the shortcomings of the current approach to avoid them in the future.

The decoding approach was mainly employing the linear SVM classification. However, the classifier was not optimized using different optimization or combining different classifiers to improve the performance as suggested by *Lotte et al.* [52]. Therefore, future BCI development may consider another more adaptive and advanced classifier, e.g., [48].

Although the decoding accuracy was higher than *Awni et al.*'s findings, the classification process was not repeated 500 times as they demonstrated. Instead, the classification was repeated only ten times inside the cross-validation due to limited computer memory and time constraint. However, this is algorithm-dependent, meaning if a better decoding algorithm was found to produce robust performance, certainly we don't need 500 times repetitions.

The decoding accuracy was not computed during ON and OFF trials because each participant did not have an insufficient and imbalanced number of trials to perform the classification. Some participants did not even have any trial left, presumably due to MW, which led to the erroneous response, and they were excluded accordingly.

7 Conclusion

The work of this thesis was developed to address the following research question:

“How many visual-spatial attention shifts can be correctly decoded from EEG and MEG data on a single trial level for future BCI applications?”

Answering this question, this thesis demonstrated a decoding algorithm using SVM classification in 10-fold cross-validation to decode the visual-spatial attention shifts, i.e., N2pc from EEG and MEG. The classifier model determined which side in the visual field the target was attended to, which cannot be performed using the conventional N2pc method. During the classification, the dataset was performed with and without STF. These processes were initially investigated at a single-trial level then increased the number of trials to create n-combined trial sets ($n=[1..10]$) for each classification and participant.

The main results revealed that the N2pc was reliable to be decoded at the single-trial level with adequate performance. A participant achieved 81.101% decoding accuracy in EEG and 81.154% in MEG. The decoding accuracy was enhanced when STF was applied, and every time the n-combined trials were increased. Ultimately, the results from MEG data and the simultaneously recorded EEG were compared, it was revealed that both decoding accuracy was not statistically significant. The focus ratings ON and OFF ratio were compared with the decodability, and they appeared not correlated. An investigation to compare the published MEG dataset by *Wienke et al.* with the current MEG dataset showed the published dataset was high in performance than the current dataset after the involvement of STF.

The work of this thesis had revealed the reliability of the decoding algorithm based on SVM classification managed to decode the visual spatial attention shifts indexed by N2pc from EEG and MEG signals in a single trial. Better decoding accuracy was influenced by STF implementation and increasing n-combined trials. However, STF enhanced the decoding accuracy better in EEG than MEG. It can also be concluded that more trials to create a combined or noise-reduced dataset were better since SNR was also increased and led to higher classification accuracy. These finding has led us to conclude that the decoding accuracy is driven by the level of N2pc effects reflected by spatial attention. The characteristics of the N2pc component in EEG/MEG can be adapted as BCI control, considering the obtained robust performance. However, the challenge is to overcome a reasonable classification time consumption, as better accuracy involves many repetitions. The stronger presence of discriminability of the relevant item from the distractors in LVF and RVF would generate reliable N2pc in a single trial ERP/ERF, which drives better decoding performance. Therefore it was possible to assume that if the decoding performance were not optimal, it could be caused by the failure of processing the stimuli by participants, meaning that the spatial attention shifts were not present. It could also be caused by MW.

Bibliography

- [1] Geoffrey F. Woodman and Steven J. Luck. Electrophysiological measurement of rapid shifts of attention during visual search. *Nature*, 400(6747):867–869, August 1999. <http://www.nature.com/articles/23698>.
- [2] Steven J. Luck and Steven A. Hillyard. Spatial filtering during visual search: Evidence from human electrophysiology. *Journal of Experimental Psychology: Human Perception and Performance*, 20(5):1000–1014, 1994. <https://doi.org/10.1037/0096-1523.20.5.1000>.
- [3] Steven J. Luck and Steven A. Hillyard. Electrophysiological correlates of feature analysis during visual search. *Psychophysiology*, 31(3):291–308, May 1994. <https://doi.org/10.1111/j.1469-8986.1994.tb02218.x>.
- [4] Christian Wienke, Mandy V Bartsch, Lena Vogelgesang, Christoph Reichert, Hermann Hinrichs, Hans-Jochen Heinze, and Stefan Dürschmid. Mind-wandering is accompanied by both local sleep and enhanced processes of spatial attention allocation. *Cerebral Cortex Communications*, 2(1), January 2021. <https://doi.org/10.1093/texcom/tgab001>.
- [5] Martin Eimer. The N2pc component as an indicator of attentional selectivity. *Electroencephalography and Clinical Neurophysiology*, 99(3):225–234, September 1996. [https://doi.org/10.1016/0013-4694\(96\)95711-9](https://doi.org/10.1016/0013-4694(96)95711-9).
- [6] Steven J. Luck, Massimo Girelli, Michele T. McDermott, and Michelle A. Ford. Bridging the gap between monkey neurophysiology and human perception: an ambiguity resolution theory of visual selective attention. *Cognitive Psychology*, 33(1):64–87, June 1997. <https://doi.org/10.1006/cogp.1997.0660>.
- [7] J.-M. Hopf. Neural sources of focused attention in visual search. *Cerebral Cortex*, 10(12):1233–1241, December 2000. <https://doi.org/10.1093/cercor/10.12.1233>.
- [8] Veronica Mazza, Massimo Turatto, and Alfonso Caramazza. Attention selection, distractor suppression and N2pc. *Cortex*, 45(7):879–890, July 2009. <https://doi.org/10.1016/j.cortex.2008.10.009>.
- [9] Hani Awini, James J.S. Norton, Stephen Umunna, Kara D. Federmeier, and Timothy Bretl. Towards a brain computer interface based on the n2pc event-related potential. *International IEEE/EMBS Conference on Neural Engineering, NER*, (1):1021–1024, 2013. <https://doi.org/10.1109/NER.2013.6696110>.
- [10] Borís Burle, Laure Spieser, Clémence Roger, Laurence Casini, Thierry Hasbroucq, and Franck Vidal. Spatial and temporal resolutions of EEG: Is it really black and white? A scalp

- current density view. *International Journal of Psychophysiology*, 97(3):210–220, September 2015. <https://doi.org/10.1016/j.ijpsycho.2015.05.004>.
- [11] P.L. Nunez, R.B. Silberstein, P.J. Cadusch, R.S. Wijesinghe, A.F. Westdorp, and R. Srinivasan. A theoretical and experimental study of high resolution EEG based on surface Laplacians and cortical imaging. *Electroencephalography and Clinical Neurophysiology*, 90(1):40–57, January 1994. [https://doi.org/10.1016/0013-4694\(94\)90112-0](https://doi.org/10.1016/0013-4694(94)90112-0).
- [12] Fabio Babiloni, Febo Cincotti, Filippo Carducci, Paolo M Rossini, and Claudio Babiloni. Spatial enhancement of EEG data by surface Laplacian estimation: the use of magnetic resonance imaging-based head models. *Clinical Neurophysiology*, 112(5):724–727, May 2001. [https://doi.org/10.1016/s1388-2457\(01\)00494-1](https://doi.org/10.1016/s1388-2457(01)00494-1).
- [13] Steven J. Luck. *An introduction to the event-related potential technique*. The MIT Press, Cambridge, Massachusetts, 2nd edition, 2014.
- [14] SanjayP Singh. Magnetoencephalography: Basic principles. *Annals of Indian Academy of Neurology*, 17(5):107, 2014. <https://doi.org/10.4103/0972-2327.128676>.
- [15] Jürgen Mellinger, Gerwin Schalk, Christoph Braun, Hubert Preissl, Wolfgang Rosenstiel, Niels Birbaumer, and Andrea Kübler. An MEG-based brain–computer interface (Bci). *NeuroImage*, 36(3):581–593, July 2007. <https://doi.org/10.1016/j.neuroimage.2007.03.019>.
- [16] Martin Spüler, Wolfgang Rosenstiel, and Martin Bogdan. Adaptive svm-based classification increases performance of a meg-based brain-computer interface(Bci). In David Hutchison, Takeo Kanade, Josef Kittler, Jon M. Kleinberg, Friedemann Mattern, John C. Mitchell, Moni Naor, Oscar Nierstrasz, C. Pandu Rangan, Bernhard Steffen, Madhu Sudan, Demetri Terzopoulos, Doug Tygar, Moshe Y. Vardi, Gerhard Weikum, Alessandro E. P. Villa, Włodzisław Duch, Péter Érdi, Francesco Masulli, and Günther Palm, editors, *Artificial Neural Networks and Machine Learning – ICANN 2012*, volume 7552, pages 669–676. Springer Berlin Heidelberg, Berlin, Heidelberg, 2012. https://doi.org/10.1007/978-3-642-33269-2_84.
- [17] F. Quandt, C. Reichert, H. Hinrichs, H.J. Heinze, R.T. Knight, and J.W. Rieger. Single trial discrimination of individual finger movements on one hand: A combined MEG and EEG study. *NeuroImage*, 59(4):3316–3324, February 2012. <https://doi.org/10.1016/j.neuroimage.2011.11.053>.
- [18] Sandra Ackerman. *Major structures and functions of the brain*. National Academies Press (US), 1992. <https://www.ncbi.nlm.nih.gov/books/NBK234157/>.
- [19] D.P. Pelvig, H. Pakkenberg, A.K. Stark, and B. Pakkenberg. Neocortical glial cell numbers in human brains. *Neurobiology of Aging*, 29(11):1754–1762, November 2008. <https://doi.org/10.1016/j.neurobiolaging.2007.04.013>.
- [20] Thuglas at English Wikipedia. The image is of Douglas Myers (Myself), i took it at Dalhousie Life Sciences Center on a research study investigating responses to startling.

- I do not care who uses the image or how, it was taken using a cell phone camera, June 2010. https://commons.wikimedia.org/wiki/File:EEG_cap.jpg, [Online; accessed 24-February-2022].
- [21] Unknown NIMH author. MEG scanner with patient from national institute of mental health., June 2009. https://commons.wikimedia.org/wiki/File:NIMH_MEG.jpg, [Online; accessed 24-February-2022].
- [22] Hans Berger. Über das elektrenkephalogramm des menschen: dritte mitteilung. *Archiv für Psychiatrie und Nervenkrankheiten*, 94(1):16–60, December 1931. <https://doi.org/10.1007/BF01835097>.
- [23] John Reaves, Timothy Flavin, Bhaskar Mitra, Mahantesh K, and Vidhyashree Nagaraju. Assessment and application of eeg: a literature review. *Journal of Applied Bioinformatics & Computational Biology*, 2021, September 2021. <https://www.scitechnol.com/abstract/an-overview-of-uptake-of-covid19-vaccine-16604.html>.
- [24] Alois Schlögl, Mel Slater, and Gert Pfurtscheller. Presence research and EEG. 2002. https://www.researchgate.net/publication/229016792_Presence_research_and_EEG.
- [25] Paul L. Nunez and Ramesh Srinivasan. *Electric fields of the brain*. Oxford University Press, January 2006. <https://doi.org/10.1093/acprof:oso/9780195050387.001.0001>.
- [26] Joachim Gross. Magnetoencephalography in cognitive neuroscience: a primer. *Neuron*, 104(2):189–204, October 2019. <https://doi.org/10.1016/j.neuron.2019.07.001>.
- [27] Peter C. Hansen, Morten L. Kringelbach, and Riitta Salmelin, editors. *MEG: an introduction to methods*. Oxford University Press, New York, 2010. OCLC: ocn502392812.
- [28] Steven J. Luck and Emily S. Kappenman. Electroencephalography and event-related brain potentials. In John T. Cacioppo, Louis G. Tassinary, and Gary G. Berntson, editors, *Handbook of Psychophysiology*, pages 74–100. Cambridge University Press, 4 edition, December 2016. <https://doi.org/10.1017/9781107415782.005>.
- [29] Wikipedia contributors. Evoked potential, 2022. https://en.wikipedia.org/w/index.php?title=Evoked_potential&oldid=1063069993, [Online; accessed 16-February-2022].
- [30] Steven A Hillyard and Marta Kutas. Event-related potentials and magnetic fields in the human brain. *Neuropsychopharmacology: the Fifth Generation of Progress*, 2002.
- [31] Steven J. Luck. *Electrophysiological correlates of the focusing of attention within complex visual scenes: n2pc and related erp components*. Oxford University Press, December 2011. <https://doi.org/10.1093/oxfordhb/9780195374148.013.0161>.
- [32] W. Grey Walter, R. Cooper, V. J. Aldridge, W. C. McCALLUM, and A. L. Winter. Contingent negative variation : an electric sign of sensori-motor association and expectancy in the human brain. *Nature*, 203(4943):380–384, July 1964. <https://doi:10.1038/203380a0>.

- [33] Geoffrey F. Woodman. A brief introduction to the use of event-related potentials in studies of perception and attention. *Attention, Perception, & Psychophysics*, 72(8):2031–2046, November 2010. <https://doi.org/10.3758/BF03196680>.
- [34] Emily S. Kappenman and Steven J. Luck. *Erp components: the ups and downs of brainwave recordings*. Oxford University Press, December 2011. <https://doi.org/10.1093/oxfordhb/9780195374148.013.0014>.
- [35] Steven J. Luck. Event-related potentials. In Harris Cooper, Paul M. Camic, Debra L. Long, A. T. Panter, David Rindskopf, and Kenneth J. Sher, editors, *APA handbook of research methods in psychology, Vol 1: Foundations, planning, measures, and psychometrics.*, pages 523–546. American Psychological Association, Washington, 2012. <https://doi.org/10.1037/13619-028>.
- [36] Samuel Sutton, Margery Braren, Joseph Zubin, and E. R. John. Evoked-potential correlates of stimulus uncertainty. *Science*, 150(3700):1187–1188, November 1965. <https://doi.org/10.1126/science.150.3700.1187>.
- [37] David E. J. Linden. The p300: where in the brain is it produced and what does it tell us? *The Neuroscientist*, 11(6):563–576, December 2005. <https://doi.org/10.1177/1073858405280524>.
- [38] John Polich. *Neuropsychology of p300*. Oxford University Press, December 2011. <https://doi.org/10.1093/oxfordhb/9780195374148.013.0089>.
- [39] L.A. Farwell and E. Donchin. Talking off the top of your head: toward a mental prosthesis utilizing event-related brain potentials. *Electroencephalography and Clinical Neurophysiology*, 70(6):510–523, December 1988. [https://doi.org/10.1016/0013-4694\(88\)90149-6](https://doi.org/10.1016/0013-4694(88)90149-6).
- [40] Marisa Carrasco. Visual attention: The past 25 years. *Vision Research*, 51(13):1484–1525, July 2011. <https://doi.org/10.1016/j.visres.2011.04.012>.
- [41] Monika Kiss, José Van Velzen, and Martin Eimer. The N2pc component and its links to attention shifts and spatially selective visual processing. *Psychophysiology*, 45(2):240–249, March 2008. <https://doi.org/10.1111/j.1469-8986.2007.00611.x>.
- [42] Steven J. Luck, Rebecca L. Fuller, Elsie L. Braun, Benjamin Robinson, Ann Summerfelt, and James M. Gold. The speed of visual attention in schizophrenia: Electrophysiological and behavioral evidence. *Schizophrenia Research*, 85(1-3):174–195, July 2006. <https://doi.org/10.1016/j.schres.2006.03.040>.
- [43] Jane W. Couperus, Kirsten O. Lydic, Juniper E. Hollis, Jessica L. Roy, Amy R. Lowe, Cindy M. Bukach, and Catherine L. Reed. Individual differences in working memory and the n2pc. *Frontiers in Human Neuroscience*, 15:620413, March 2021. <https://doi.org/10.3389/fnhum.2021.620413>.

- [44] Emily S. Kappenman, Jaclyn L. Farrens, Wendy Zhang, Andrew X. Stewart, and Steven J. Luck. ERP CORE: An open resource for human event-related potential research. *NeuroImage*, 225:117465, January 2021. <https://doi.org/10.1016/j.neuroimage.2020.117465>.
- [45] Jason Brownlee. 4 types of classification tasks in machine learning, April 2020. <https://machinelearningmastery.com/types-of-classification-in-machine-learning/>, [Online; accessed 19-February-2022].
- [46] Trevor Hastie, Robert Tibshirani, and J. H. Friedman. *The elements of statistical learning: data mining, inference, and prediction*. Springer series in statistics. Springer, New York, NY, 2nd ed edition, 2009.
- [47] Jonathan R Wolpaw, Niels Birbaumer, Dennis J McFarland, Gert Pfurtscheller, and Theresa M Vaughan. Brain-computer interfaces for communication and control. *Clinical Neurophysiology*, 113(6):767–791, June 2002. [https://doi.org/10.1016/S1388-2457\(02\)00057-3](https://doi.org/10.1016/S1388-2457(02)00057-3).
- [48] F Lotte, L Bougrain, A Cichocki, M Clerc, M Congedo, A Rakotomamonjy, and F Yger. A review of classification algorithms for EEG-based brain-computer interfaces: a 10 year update. *Journal of Neural Engineering*, 15(3):031005, June 2018. <https://doi.org/10.1088/1741-2552/aab2f2>.
- [49] A. Kubler, F. Nijboer, J. Mellinger, T. M. Vaughan, H. Pawelzik, G. Schalk, D. J. McFarland, N. Birbaumer, and J. R. Wolpaw. Patients with ALS can use sensorimotor rhythms to operate a brain-computer interface. *Neurology*, 64(10):1775–1777, May 2005. <https://doi.org/10.1212/01.WNL.0000158616.43002.6D>.
- [50] G. Pfurtscheller, G.R. Muller-Putz, R. Scherer, and C. Neuper. Rehabilitation with brain-computer interface systems. *Computer*, 41(10):58–65, October 2008. <https://doi.org/10.1109/MC.2008.432>.
- [51] Kai Keng Ang and Cuntai Guan. Brain-computer interface in stroke rehabilitation. *Journal of Computing Science and Engineering*, 7(2):139–146, 2013. <https://doi.org/10.5626/JCSE.2013.7.2.139>.
- [52] F Lotte, M Congedo, A Lécuyer, F Lamarche, and B Arnaldi. A review of classification algorithms for EEG-based brain-computer interfaces. *Journal of Neural Engineering*, 4(2):R1–R13, June 2007. <https://doi:10.1088/1741-2560/4/2/R01>.
- [53] Christopher J.C. Burges. A Tutorial on Support Vector Machines for Pattern Recognition. *Data Mining and Knowledge Discovery*, 2(2):121–167, 1998. <https://doi.org/10.1023/A:1009715923555>.
- [54] Harold Hotelling. Relations between two sets of variates. *Biometrika*, 28(3/4):321, December 1936. <https://doi.org/10.2307/2333955>.

- [55] Christoph Reichert, Stefan Dürschmid, Rudolf Kruse, and Hermann Hinrichs. An efficient decoder for the recognition of event-related potentials in high-density meg recordings. *Computers*, 5(2):5, April 2016. <https://doi.org/10.3390/computers5020005>.
- [56] Martin Spuler, Armin Walter, Wolfgang Rosenstiel, and Martin Bogdan. Spatial filtering based on canonical correlation analysis for classification of evoked or event-related potentials in eeg data. *IEEE Transactions on Neural Systems and Rehabilitation Engineering*, 22(6):1097–1103, November 2014. <https://doi.org/10.1109/TNSRE.2013.2290870>.
- [57] Guangyu Bin, Xiaorong Gao, Zheng Yan, Bo Hong, and Shangkai Gao. An online multi-channel SSVEP-based brain–computer interface using a canonical correlation analysis method. *Journal of Neural Engineering*, 6(4):046002, August 2009. <https://doi.org/10.1088/1741-2560/6/4/046002>.
- [58] Cyril R. Pernet, Paul Sajda, and Guillaume A. Rousselet. Single-trial analyses: why bother? *Frontiers in Psychology*, 2, 2011. <https://doi.org/10.3389/fpsyg.2011.00322>.
- [59] Benjamin Blankertz, Steven Lemm, Matthias Treder, Stefan Haufe, and Klaus-Robert Müller. Single-trial analysis and classification of ERP components — A tutorial. *NeuroImage*, 56(2):814–825, May 2011. <https://doi:10.1016/j.neuroimage.2010.06.048>.
- [60] Martin Eimer. The neural basis of attentional control in visual search. *Trends in Cognitive Sciences*, 18(10):526–535, October 2014. <https://doi.org/10.1016/j.tics.2014.05.005>.
- [61] Veronica Mazza and Alfonso Caramazza. Temporal brain dynamics of multiple object processing: the flexibility of individuation. *PLoS ONE*, 6(2):e17453, February 2011. <https://doi.org/10.1371/journal.pone.0017453>.
- [62] J.-M. Hopf. Attention to features precedes attention to locations in visual search: evidence from electromagnetic brain responses in humans. *Journal of Neuroscience*, 24(8):1822–1832, February 2004. <https://doi.org/10.1523/JNEUROSCI.3564-03.2004>.
- [63] Johannes Jacobus Fahrenfort, Anna Grubert, Christian N. L. Olivers, and Martin Eimer. Multivariate EEG analyses support high-resolution tracking of feature-based attentional selection. *Scientific Reports*, 7(1):1886, December 2017. <https://doi.org/10.1038/s41598-017-01911-0>.
- [64] Christoph Reichert, Stefan Dürschmid, Mandy V Bartsch, Jens-Max Hopf, Hans-Jochen Heinze, and Hermann Hinrichs. Decoding the covert shift of spatial attention from electroencephalographic signals permits reliable control of a brain-computer interface. *Journal of Neural Engineering*, 17(5):056012, October 2020. <https://doi.org/10.1088/1741-2552/abb692>.
- [65] Christoph Reichert, Igor Fabian Tellez Ceja, Catherine M. Sweeney-Reed, Hans-Jochen Heinze, Hermann Hinrichs, and Stefan Dürschmid. Impact of stimulus features on the performance of a gaze-independent brain-computer interface based on covert spatial attention

- shifts. *Frontiers in Neuroscience*, 14:591777, December 2020. <https://doi.org/10.3389/fnins.2020.591777>.
- [66] Christoph Reichert, Stefan Dürschmid, Hans-Jochen Heinze, and Hermann Hinrichs. A comparative study on the detection of covert attention in event-related eeg and meg signals to control a bci. *Frontiers in Neuroscience*, 11:575, October 2017. <https://doi.org/10.3389/fnins.2017.00575>.
- [67] Martin Eimer and Monika Kiss. Involuntary attentional capture is determined by task set: evidence from event-related brain potentials. *Journal of Cognitive Neuroscience*, 20(8):1423–1433, August 2008. <https://doi.org/10.1162/jocn.2008.20099>.
- [68] S. Taulu, J. Simola, and M. Kajola. Applications of the signal space separation method. *IEEE Transactions on Signal Processing*, 53(9):3359–3372, September 2005. <https://doi.org/10.1109/TSP.2005.853302>.
- [69] Mainak Jas. Raw data, 2019. https://jasmainak.github.io/mne-workshop-brown/raw_to_evoked/raw.html.
- [70] Alain de Cheveigné and Israel Nelken. Filters: when, why, and how (Not) to use them. *Neuron*, 102(2):280–293, April 2019. <https://doi.org/10.1016/j.neuron.2019.02.039>.
- [71] Ramesh Srinivasan, Don M. Tucker, and Michael Murias. Estimating the spatial Nyquist of the human EEG. *Behavior Research Methods, Instruments, & Computers*, 30(1):8–19, March 1998. <https://doi.org/10.3758/BF03209412>.
- [72] John W Leis. *Digital signal processing using MATLAB for students and researchers*. Wiley, Hoboken, N.J., 2011. <https://www.wiley.com/en-au/Digital+Signal+Processing+Using+MATLAB+for+Students+and+Researchers-p-9780470880913>.
- [73] J.-M. Hopf. The neural site of attention matches the spatial scale of perception. *Journal of Neuroscience*, 26(13):3532–3540, March 2006. <https://doi.org/10.1523/JNEUROSCI.4510-05.2006>.
- [74] Sarah E. Donohue, Jens-Max Hopf, Mandy V. Bartsch, Mircea A. Schoenfeld, Hans-Jochen Heinze, and Marty G. Woldorff. The rapid capture of attention by rewarded objects. *Journal of Cognitive Neuroscience*, 28(4):529–541, April 2016. https://doi.org/10.1162/jocn_a_00917.
- [75] J.-M Hopf, K Boelmans, A.M Schoenfeld, H.-J Heinze, and S.J Luck. How does attention attenuate target–distractor interference in vision? *Cognitive Brain Research*, 15(1):17–29, December 2002. [https://doi.org/10.1016/S0926-6410\(02\)00213-6](https://doi.org/10.1016/S0926-6410(02)00213-6).
- [76] Jochem W. Rieger, Christoph Reichert, Karl R. Gegenfurtner, Toemme Noesselt, Christoph Braun, Hans-Jochen Heinze, Rudolf Kruse, and Hermann Hinrichs. Predicting the recognition of natural scenes from single trial MEG recordings of brain activity. *NeuroImage*, 42(3):1056–1068, September 2008. <https://doi.org/10.1016/j.neuroimage.2008.06.014>.

- [77] Vladimir N. Vapnik. *The nature of statistical learning theory*. Springer New York, New York, NY, 1995. <https://doi:10.1007/978-1-4757-2440-0>.
- [78] Trevor Hastie, Saharon Rosset, Robert Tibshirani, and Ji Zhu. The entire regularization path for the support vector machine. *The Journal of Machine Learning Research*, 5:1391–1415, December 2004. <http://jmlr.org/papers/volume5/hastie04a/hastie04a.pdf>.
- [79] Thorsten Joachims. *Learning to classify text using support vector machines*. Springer US, Boston, MA, 2002. <https://doi.org/10.1007/978-1-4615-0907-3>.
- [80] Bernhard Schoelkopf, Christopher J. C. Burges, and Alexander J. Smola, editors. *Advances in kernel methods: support vector learning*. MIT Press, Cambridge, Mass, 1999. <http://cognet.mit.edu/book/advances-kernel-methods>.
- [81] Gareth James, Daniela Witten, Trevor Hastie, and Robert Tibshirani, editors. *An introduction to statistical learning: with applications in R*. Number 103 in Springer texts in statistics. Springer, New York, 1 edition, 2013. <https://link.springer.com/book/10.1007/978-1-4614-7138-7>.
- [82] Christoph Reichert, Igor F. Tellez Ceja, and Stefan Dürschmid. Spatial attention shifts to colored items - an EEG-based brain-computer interface. 2020. <https://doi.org/10.24352/UB.OVGU-2020-155>, Type: dataset.
- [83] Joos Korstanje. The F1 score, August 2021. <https://towardsdatascience.com/the-f1-score-bec2bbc38aa6>, [Online; accessed 28-February-2022].
- [84] Wikipedia contributors. Confusion matrix, December 2021. https://en.wikipedia.org/w/index.php?title=Confusion_matrix&oldid=1058352752, [Online; accessed 28-February-2022].
- [85] JASP Team. JASP (Version 0.16)[Computer software], 2021. <https://jasp-stats.org/>.
- [86] Ioannis Delis, Arno Onken, Philippe G. Schyns, Stefano Panzeri, and Marios G. Philiastides. Space-by-time decomposition for single-trial decoding of M/EEG activity. *NeuroImage*, 133:504–515, June 2016. <https://doi.org/10.1016/j.neuroimage.2016.03.043>.
- [87] Francisco Pereira, Tom Mitchell, and Matthew Botvinick. Machine learning classifiers and fMRI: A tutorial overview. *NeuroImage*, 45(1):S199–S209, March 2009. <https://doi.org/10.1016/j.neuroimage.2008.11.007>.
- [88] Marios G. Philiastides and Paul Sajda. Temporal characterization of the neural correlates of perceptual decision making in the human brain. *Cerebral Cortex*, 16(4):509–518, April 2006. <https://doi.org/10.1093/cercor/bhi130>.
- [89] Alex Brandmeyer, Makiko Sadakata, Loukianos Spyrou, James M. McQueen, and Peter Desain. Decoding of single-trial auditory mismatch responses for online perceptual monitoring and neurofeedback. *Frontiers in Neuroscience*, 7, 2013. <https://doi.org/10.3389/fnins.2013.00265>.

- [90] Mohammad Reza Nazari, Ali Motie Nasrabadi, and Mohammad Reza Daliri. Single-trial decoding of motion direction during visual attention from local field potential signals. *IEEE Access*, 9:66450–66461, 2021. <https://doi.org/10.1109/ACCESS.2021.3076865>.
- [91] Michał Bola, Marta Paź, Łucja Doradzińska, and Anna Nowicka. The self-face captures attention without consciousness: Evidence from the N2pc ERP component analysis. *Psychophysiology*, 58(4), April 2021. <https://doi.org/10.1111/psyp.13759>.
- [92] Orestis Papaioannou and Steven J. Luck. Effects of eccentricity on the attention-related N2pc component of the event-related potential waveform. *Psychophysiology*, 57(5), May 2020. <https://doi.org/10.1111/psyp.13532>.
- [93] Veronica Mazza, Massimo Turatto, and Alfonso Caramazza. An electrophysiological assessment of distractor suppression in visual search tasks. *Psychophysiology*, 46(4):771–775, July 2009. <https://doi.org/10.1111/j.1469-8986.2009.00814.x>.
- [94] Greta Tuckute, Sofie Therese Hansen, Nicolai Pedersen, Dea Steenstrup, and Lars Kai Hansen. Single-trial decoding of scalp eeg under natural conditions. *Computational Intelligence and Neuroscience*, 2019:1–11, April 2019. <https://doi.org/10.1155/2019/9210785>.
- [95] Sarah E. Donohue, Mircea A. Schoenfeld, and Jens-Max Hopf. Parallel fast and slow recurrent cortical processing mediates target and distractor selection in visual search. *Communications Biology*, 3(1):689, December 2020. <https://doi.org/10.1038/s42003-020-01423-0>.
- [96] Mark F. Bear, Barry W. Connors, and Michael A. Paradiso. *Neuroscience: exploring the brain*. Wolters Kluwer, Philadelphia, 4th edition, 2016.
- [97] Jeffrey S. Kreutzer, John DeLuca, and Bruce Caplan, editors. *Encyclopedia of clinical neuropsychology*. Springer New York, New York, NY, 2011. <https://doi.org/10.1007/978-0-387-79948-3>.
- [98] Robert M. Stelmack, editor. *On the psychobiology of personality*. Elsevier, 2004. <https://doi.org/10.1016/B978-0-08-044209-9.X5000-3>.

Appendix

Table A.1: Decoding Accuracies of 13 Participants at Single-trial Level (n=1)

Participants	EEG	MEG	EEG (STF)	MEG (STF)
1	58.182	58.739	54.432	51.773
2	70.56	61.731	76.662	55.57
3	74.274	73.325	82.781	78.612
4	73.474	68.875	77.792	70.057
5	70.891	71.693	78.337	76.455
6	81.101	81.154	83.411	88.287
7	64.433	69.205	67.383	72.793
8	73.453	79.389	82.374	84.433
9	73.802	73.348	82.057	77.631
10	54.07	52.603	53.539	53.278
11	60.272	66.233	72.697	60.424
12	64.428	77.116	72.749	79.119
13	64.116	62.229	67.505	55.235
Mean	67.927	68.895	73.209	69.513
SD	7.692	8.4	10.098	12.697

Table A.2: Decoding Accuracies of 13 Participants (n=2)

Participants	EEG	MEG	EEG (STF)	MEG (STF)
1	59.705	63.33	63.568	67.318
2	75.709	65.552	82.785	74.147
3	79.392	81.025	87.347	85.64
4	79.222	73.264	84.84	74.556
5	77.228	76.851	84.366	82.871
6	88.751	87.97	90.666	94.697
7	67.368	74.98	73.428	77.422
8	81.611	85.699	88.432	91.636
9	81.883	79.074	87.781	84.142
10	55.436	52.43	57.144	56.204
11	63.514	66.485	75.009	70.302
12	70.141	83.709	79.189	85.606
13	68.118	67.38	71.329	66.584
Mean	72.929	73.673	78.914	77.779
SD	9.767	10.249	10.29	10.983

Table A.3: Decoding Accuracies of 13 Participants (n=3)

Participants	EEG	MEG	EEG (STF)	MEG (STF)
1	61.193	65.08	64.614	70.42
2	81.102	69.808	87.847	78.617
3	84.981	85.81	91.486	89.38
4	84.313	79.108	88.964	79.369
5	82.921	82.04	90.188	88.02
6	93.129	92.493	94.409	97.536
7	72.411	80.18	78.024	81.251
8	86.57	89.684	92.523	94.47
9	86.959	85.09	93.168	88.781
10	58.232	52.041	57.403	57.543
11	69.714	72.28	78.71	74.092
12	74.035	89.694	84.639	90.018
13	72.922	72.052	75.346	69.176
Mean	77.576	78.105	82.871	81.436
SD	10.477	11.521	11.563	11.445

Table A.4: Decoding Accuracies of 13 Participants (n=4)

Participants	EEG	MEG	EEG (STF)	MEG (STF)
1	64.955	68	67.67	73.216
2	84.983	71.108	90.815	81.899
3	88.418	89.035	93.368	91.856
4	87.362	82.115	92.334	81.854
5	86.109	85.366	92.574	90.208
6	95.535	94.995	96.719	98.816
7	75.464	84.497	81.399	84.906
8	89.265	93.434	94.785	97.051
9	90.442	88.804	95.678	91.949
10	59.202	52.976	58.846	60.026
11	70.219	75.28	82.037	75.745
12	77.522	92.663	87.835	93.133
13	75.45	73.341	77.779	72.67
Mean	80.379	80.893	85.526	84.102
SD	10.892	12.206	11.636	11.306

Table A.5: Decoding Accuracies of 13 Participants (n=5)

Participants	EEG	MEG	EEG (STF)	MEG (STF)
1	65.682	69.989	69.739	76.489
2	87.684	74.083	92.763	84.238
3	91.089	90.688	95.334	93.908
4	89.457	84.324	94.195	84.352
5	88.089	88.03	94.069	91.683
6	97.528	97.353	97.912	99.422
7	78.029	86.296	83.529	87.423
8	91.428	95.265	96.264	98.034
9	92.475	90.738	97.621	93.018
10	58.723	53.356	59.82	58.448
11	73.977	76.779	83.108	78.409
12	80.978	94.674	89.624	94.561
13	77.602	76.541	81.099	75.922
Mean	82.518	82.932	87.314	85.839
SD	11.374	12.442	11.642	11.397

Table A.6: Decoding Accuracies of 13 Participants (n=6)

Participants	EEG	MEG	EEG (STF)	MEG (STF)
1	67.295	70.625	71.784	78.716
2	88.949	75.811	94.223	85.104
3	92.942	93.017	96.424	95.412
4	91.295	87.43	96.13	86.276
5	90.673	89.356	95.812	93.139
6	98.431	97.834	98.624	99.74
7	80.596	89.117	85.966	89.347
8	93.143	96.237	97.48	98.56
9	94.834	92.923	98.275	94.777
10	61.076	53.501	59.946	60.992
11	75.083	78.946	86.049	79.141
12	82.844	95.61	91.727	96.227
13	80.331	79.5	83.078	76.482
Mean	84.422	84.608	88.886	87.224
SD	11.253	12.651	11.658	11.092

Table A.7: Decoding Accuracies of 13 Participants (n=7)

Participants	EEG	MEG	EEG (STF)	MEG (STF)
1	69.114	73.261	73.114	80.341
2	91.051	77.175	96.109	86.764
3	94.118	93.709	97.094	96.417
4	92.528	88.787	96.682	87.879
5	92.228	91.287	96.743	94.515
6	98.98	98.806	99.163	99.875
7	82.805	91.046	88.027	90.425
8	94.329	97.368	97.841	99.125
9	95.53	95.018	98.781	95.779
10	61.553	53.54	59.67	62.081
11	76.731	81.206	87.214	81.335
12	84.665	97.277	93.424	97.016
13	82.193	80.577	83.796	78.05
Mean	85.833	86.081	89.82	88.431
SD	11.167	12.808	11.786	10.797

Table A.8: Decoding Accuracies of 13 Participants (n=8)

Participants	EEG	MEG	EEG (STF)	MEG (STF)
1	69.273	74.364	74.716	80.852
2	92.514	79.115	96.479	88.542
3	95.49	95.081	97.954	97.399
4	94.069	90.119	97.448	88.709
5	93.554	92.208	97.644	95.277
6	99.384	99.153	99.432	99.952
7	83.785	92.268	89.818	91.451
8	95.905	97.834	98.706	99.426
9	96.551	95.851	99.197	96.374
10	62.231	54.849	61.127	62.435
11	77.174	83.484	88.464	81.627
12	85.972	97.806	94.256	97.996
13	81.778	83.095	85.262	80.315
Mean	86.745	87.325	90.808	89.258
SD	11.48	12.49	11.439	10.729

Table A.9: Decoding Accuracies of 13 Participants (n=9)

Participants	EEG	MEG	EEG (STF)	MEG (STF)
1	69.557	74.807	75.034	81.58
2	93.491	80.034	96.465	90.186
3	96.088	96.022	98.124	97.641
4	94.546	91.178	98.362	90.228
5	95.099	93.436	98.168	95.822
6	99.682	99.24	99.74	99.971
7	85.048	93.856	90.74	92.488
8	96.403	98.274	99.028	99.659
9	96.878	96.941	99.148	97.327
10	61.691	55.531	61.871	64.053
11	80.951	83.483	90.441	81.476
12	86.985	98.243	94.784	97.736
13	83.899	83.686	86.556	79.89
Mean	87.717	88.056	91.42	89.85
SD	11.483	12.536	11.288	10.502

Table A.10: Decoding Accuracies of 13 Participants (n=10)

Participants	EEG	MEG	EEG (STF)	MEG (STF)
1	70.977	75.489	76.75	81.807
2	94.295	81.638	97.291	91.327
3	96.475	96.233	98.428	97.945
4	94.94	91.553	98.372	90.706
5	95.386	93.842	98.416	96.762
6	99.731	99.654	99.769	99.99
7	86.116	94.348	91.987	93.533
8	96.724	98.838	99.242	99.747
9	97.533	97.626	99.653	97.545
10	63.328	55.347	62.569	64.687
11	80.8	84.863	90.801	84.918
12	87.368	98.817	95.448	98.605
13	85.24	85.687	87.421	81.988
Mean	88.378	88.764	92.011	90.735
SD	11.101	12.545	11.013	10.166

Table A.11: Parieto-occipital channels of EEG and the corresponding N2pc period. The temporal N2pc activity was defined by the significant difference between contralateral and ipsilateral waveforms (grey shade in Figure 5.6a)

EEG Channels		Significant Difference	
Left Hemisphere	Right Hemisphere	Start Period	End Period
P3	-	P4	178ms
O9	-	O10	218ms
P7	-	P8	188ms
CP1	-	CP2	214ms
PO3	-	PO4	178ms
PO7	-	PO8	180ms